Optimization of Triple-Pressure Combined-Cycle Power Plants by Generalized Disjunctive Programming and Extrinsic Functions.

Juan I. Manassaldi [1], Miguel C. Mussati [1,2], Nicolás J. Scenna [1], Sergio F. Mussati [1,2] *

[1] CAIMI, UTN FRRo, Zeballos 1341, S2000BQA, Rosario, Argentina, Tel.: +54 341 4480102,

[2] INGAR (CONICET-UTN) - Instituto de Desarrollo y Diseño, Avellaneda 3657, 3000, Santa Fe, Argentina, Tel.: +54 342 4534451, Fax: +54 342 4553439

jmanassaldi@frro.utn.edu.ar, mmussati@santafe-conicet.gov.ar, nscenna@santafe-conicet.gov.ar, mussati@santafe-conicet.gov.ar

* Corresponding author

Abstract:

A new mathematical framework for optimal synthesis, design, and operation of triple-pressure steam-reheat combined-cycle power plants (CCPP) is presented. A superstructure-based representation of the process, which embeds a large number of candidate configurations, is first proposed. Then, a generalized disjunctive programming (GDP) mathematical model is derived from it. Series, parallel, and combined series-parallel arrangements of heat exchangers are simultaneously embedded. Extrinsic functions executed outside GAMS from dynamic-link libraries (DLL) are used to estimate the thermodynamic properties of the working fluids. As a main result, improved process configurations with respect to two reported reference cases were found. The total heat transfer areas calculated in this work are by around 15% and 26% lower than those corresponding to the reference cases.

This paper contributes to the literature in two ways: (i) with a disjunctive optimization model of natural gas CCPP and the corresponding solution strategy, and (ii) with improved HRSG configurations.

Keywords: Generalized Disjunctive Programming; Extrinsic Functions; Three-Pressure Reheat Combined-Cycle Power Plant; Heat Recovery Steam Generator HRSG; GAMS.

.

1. Introduction

Combined cycle power plants (CCPP) are widely used industrial plants or larger distribution networks to provide both electricity and heat as energy vectors. The overall thermal efficiency of combined-cycle power plants (CCPPs) depends strongly on the gas and steam turbine technologies as well as the configuration and design of the heat recovery steam generators (HRSGs). Improved CCPPs lead to reduce fuel consumption and, consequently, the greenhouse gas emissions. The configuration, design, and operating conditions of HRSGs are critical because they couple the gas turbine-based topping cycle with the steam turbine-based bottoming cycle. The exhaust waste energy of gas turbines can be recovered in HRSGs using different reheat cycles: from a single-pressure to triple-pressure cycles. In a CCPP, the optimal configuration of the HRSG depends strongly on the desired level of electricity to be generated, and, if it is the case, on the amount of steam required as utility heating if the CCPP is integrated to an industrial plant. Therefore, it is of great interest to still study the optimization of CCPPs through detailed process models and simultaneous optimization methods (Blumberg et al., 2017; Nadir and Ghenaiet, 2015), as it is proposed in this paper.

There are many published papers addressing the mathematical modeling and optimization of combined heat and power (CHP) generation systems, which differ in the criteria used to solve the resulting mathematical models (energy, exergy, cost, exergo-economic analyses, simulation-based optimization, simultaneous optimization, or meta-heuristic approaches), the number of optimization criteria (single or multi-objective optimization), and/or the model assumptions and design specifications considered for the analysis (fixed or variable process configurations, fixed or variable number of pressure levels, fixed or variable amount of steam and/or electricity to be generated).

Exergy and exergo-economic analyses of energy conversion systems to systematically locate the most inefficient system components have been used as a valuable decision-making tool (Bracco and Siri, 2010; Boyaghchi and Molaie, 2015; Bakhshmand et al., 2015; Tsatsaronis and Park, 2002; Morosuk and Tsatsaronis, 2011; Tsatsaronis, 1999; Sahoo, 2008; Ahmadi and Dincer, 2011). For instance, the retrofit of an already existing process can be improved by switching out and/or introducing new components towards a lower value of the total irreversibility of the system. These analyses are iterative in nature and contribute to improving a thermal system as a whole or at a component level. Although the calculation of exergy is more complex than the calculation of energy, the exergy analysis allows quantifying more accurately the types, causes, and locations of inefficiencies. Bakhshmand et al. (2015) performed an exergo-economic analysis and optimization of a triple-pressure combined cycle. To do this, they implemented a simulation code in MATLAB using an evolutionary algorithm. The objective function included both product cost rate and cost rates associated with exergy destruction. The obtained results allowed to propose optimal performance criteria for the studied process. The authors highlighted that this methodology is applicable to optimize steady state operation parameters of a given combined cycle, but it is not suitable to optimize the design of new cycles. Tsatsaronis and Park (2002) and Morosuk and Tsatsaronis (2011) concluded about the advantages of dividing exergy destruction and economic costs into avoidable and unavoidable parts in cogeneration plants (Tsatsaronis and Park, 2002) and simple gas turbine systems

(Morosuk and Tsatsaronis, 2011), showing the potential for improvement and the interactions among the system components. In exergy analyses, structural coefficients are used to consider how the overall irreversibility of the cycle is influenced by the local irreversibilities of each component. These structural coefficients can be calculated once the irreversibilities of the components and the whole cycle are known. Therefore, in a system with many components with a large number of discrete decisions, the calculation of these coefficients may require a high number of simulation runs resulting in a time-consuming procedure (Tsatsaronis, 1999). Most exergy and exergo-economic optimization approaches are subjective in nature as they require the designer's interpretation at each iteration to find the final configuration (Sahoo, 2008).

On the other hand, the degree of development of the optimization methods and software, and the availability of powerful computational systems have motivated a renewed interest in applying evolutionary algorithms, mathematical programming techniques in industry, including utility plants and CHP systems.

Applications of evolutionary algorithms – such as simulated annealing (SA) and genetic algorithms (GA) – can be found in Ahmadi and Dincer, 2011; Ahmadi et al., 2012; Kaviri et al., 2012; Mehrpanahi et al., 2019; Ameri et al., 2018; Mehrgoo et al., 2017; Naserabad et al., 2018; Rezaie et al., 2019). These algorithms have been successfully applied for optimization of power plants with known (fixed) configurations. GAs and derivative-free algorithms are well suitable when no information is available about the gradient of the function at the evaluated points. As GAs can be parallelized with little effort, a lot of paths to the optimum are considered in parallel, which is important in high-complexity problems with many solutions. However, GAs require many parameters, such as the number of generations, population, crossover and mutation rates, and tournament size (number of individuals needed to fill a tournament during selection) that can significantly affect the obtained solutions.

The use of advanced optimization methods and the development of rigorous mathematical models made possible to find new HRSG configurations with the corresponding optimal operating conditions. In this context, there are several articles addressing the study of energy systems, including power and heat plants, which employ gradient-based optimization algorithms and deterministic mixed-integer nonlinear programming techniques (MINLP). The use of MINLP techniques for some representative applications can be found in Kim and Edgar (2014) and particularly in Gopalakrishnan and Kosanovic (2015) for optimal scheduling of CHP plants, in Santos and Urtubey (2018) for optimal energy dispatch in cogeneration plants, in Elsido et al. (2017) for optimal design of organic Rankine cycles (ORC), and in Perez-Uresti et al. (2019) for optimal design of renewable-based utility plants.

Other applications include the design of supercritical coal-fired power plants (Wang et al., 2014), short-term planning of cogeneration power plants (Taccari et al., 2015; Bruno et al., 1998), optimal synthesis and design of single and/or dual-purpose seawater desalination plants (Tanvir and Mujtaba, 2008; Mussati et al., 2003a; Mussati et al., 2003b; Mussati et al., 2004; Mussati et al., 2005), as well as optimal integration of natural gas combined cycle (NGCC) power plants and CO_2 capture plants (Manassaldi et al., 2014; Mores et al., 2018). Also, MINLP models were successfully applied in other areas such as design of water and wastewater treatment processes (Lu et al., 2017; Faria and Bagajewicz, 2012; Ahmetovic and Grossmann, 2011), heat exchanger network in fuel processing systems for PEM fuel cells (Oliva et al., 2011), design and dispatch of SOFC-based CCHP system (Jing et al., (2017), scheduling and retrofit of refinery preheat trains (Izyan et al., 2014), among other applications. Leon and Martin (2016) addressed the optimization of a combined cycle power plant by considering biogas as fuel. To this end, the authors implemented a mixed integer nonlinear programming (MINLP) model in GAMS and investigated two alternative schemes for the steam production. The calculation of the thermodynamics for the steam was included in the model via surrogate models. Although MINLP formulations are in general hard to solve (especially when the feasible regions are non-convex), they are the most suitable alternative for highly nonlinear and combinatorial optimization problems and large-size mathematical models (problems involving many discrete and continuous decisions and nonlinear equality constraints). In this work, due to the characteristics of the proposed optimization models, the MINLP technique is used.

Despite the existence of many articles concerning with the study of NGCC power plants under different assumptions and using different computational tools, only a few papers considering the simultaneous optimization of the HRSG configuration, process-unit sizes, and operating conditions can be found in literature (Ahadi-Oskui et al., 2010, Martelli et al., 2017; Zhang et al., 2014; Manassaldi et al., 2016; Franco and Giannini, 2006). Ahadi-Oskui et al. (2010) applied mathematical programming methods to simultaneously optimize the configuration and operating conditions of a combined-cycle-based cogeneration plant. To this end, the authors formulated a nonconvex mixed-integer nonlinear problem (MINLP). The resulting model was successfully solved by using their own MINLP solver called LaGO which generates a convex relaxation of the MINLP and applies a Branch and Cut algorithm to the relaxation. Martelli et al. (2017) proposed a two-stage methodology to optimize HRSGs of simple CHP cycles considering external heat/steam sources/users with the possibility of multiple supplementary firing. The proposed methodology was clearly described through an integrated gasification combined cycle (IGCC) plant with CO_2 capture. Zhang et al. (2014) proposed a superstructure-based MINLP model to optimize the configuration of a HRSG embedding several candidate matches between the HRSG and external heat flows. The resulting model is non-convex because of the presence of bilinear terms. The solver BARON (Branch-And-Reduce Optimization Navigator) (Sahinidis, 2000), which is supported in GAMS (General Algebraic Modeling System) (Brooke et al., 1992), was used as a global optimizer. Several case studies considering different pressure levels, with and without steam reheating, were successfully solved. Franco and Giannini (2006) proposed a two-level optimization framework of HRSGs. The former level consists on obtaining the main operating conditions, and the second one the detailed design of each section (sizes and geometric variables). The framework uses the optimal output of the first level as the input to the second level. The authors successfully verified the proposed framework using already existing HRSG structures. Also, simultaneous optimization has been successfully applied to other integrated systems such as biomass Fischer-Tropsch liquids plants. Manassaldi et al. (2016) proposed a discrete and continuous mathematical model to optimize the synthesis and design of dual-pressure HRSGs coupled to two steam turbines. The optimization problem consisted in determining how the heat exchangers (economizers, evaporators, and superheaters) should be connected in the HRSG to maximize the total net power keeping fixed the total heat transfer area, or either to minimize the total heat transfer area keeping fixed the total net power. Also, the optimal operating conditions and size of each process unit were determined simultaneously. The resulting MINLP problem was solved using SBB (Standard Branch and Bound) (Bussieck and Drud, 2001) and the solver CONOPT for the nonlinear problems (NLP) (Drud, 1992). The authors found a novel HRSG configuration not previously reported in the literature. Recently, Bongartz et al. (2020) discussed three bottoming cycles for combined cycle power plants of increasing complexity. The authors employed their open-source deterministic global solver MAiNGO and developed a novel method for constructing relaxations of the functions reported in IAPWS-IF97 to calculate the thermodynamic properties of water and steam. The relaxations were implemented in the MC++ library (https://omega-icl.github.io/mcpp/index.html). The authors concluded that the proposed relaxations considerably reduce the computational time required to find the global optimal solution with respect to McCormick relaxations.

Generalized disjunctive programming (GDP) is an alternative modeling framework to represent optimization problems with discrete and continuous decisions (Chen and Grossmann, 2019). In GDP formulations, discrete decisions are represented in a natural way through the use of disjunctions in the continuous space and logic propositions in the discrete space which are then relaxed, obtaining a MINLP problem (Lee and Grossmann, 2000). GDPs can be reformulated via the convex hull (Grossmann and Lee, 2003) or via Big-M formulations (Grossmann and Ruiz, 2012). Vecchietti et al.

(2003) developed the computer code LogMIP to solve discrete/continuous nonlinear optimization problems that are modeled with either algebraic, disjunctive, or hybrid formulations.

This paper is a natural continuation of the work presented by Manassaldi et al. (2016). Here, the superstructure-based model developed by Manassaldi et al. (2016) is used as a basis and it is properly extended to include three pressure levels as well as more candidate process configurations, thus highly increasing the combinatorial nature of the resulting superstructure-based optimization model. From a qualitative point of view, the main differences between this work and that of Manassaldi et al. (2016) are: (a) the type of the combined cycle to be studied (the inclusion of a third pressure level significantly increases the degrees of freedom for the optimization problems), (b) the mathematical modeling strategy (a generalized disjunctive programming (GDP) model is formulated instead of a pure MINLP model), and (c) the solution strategy includes a dynamic-link library (DLL) to estimate the thermodynamic properties of both circulating fluids (flue gas and water) at different conditions (in the case of water as subcooled and saturated liquid, saturated and superheated steam). On the other hand, the main difference between this work and papers published by other authors is the obtaining of improved configurations for a triple-pressure HRSG. Thus, to the best of our knowledge, this paper contributes to the literature of this field in two ways: (i) with a mathematical optimization model of NGCC power plants operated at three pressure levels and the corresponding solution strategy, and (ii) with improved HRSG configurations with respect to reference configurations taken from the literature.

The paper is organized as follows. Section 2 describes the process superstructure representation. Section 3 defines the problem statement. Section 4 presents the mathematical model. Section 5 discusses the obtained results. Finally, Section 6 provides the conclusions of the investigation.

2. Process superstructure representation

As mentioned earlier, the heat exchangers in a HRSG operating at three pressure levels can be arranged in different ways. Also, the inlet of the working fluid in the HRSG can be located in the low-pressure (LP) level, or in the LP and medium-pressure (MP) levels, or in the LP, MP and high (HP) pressure levels. As an illustration, Fig. 1 presents three candidate configurations, which differ in the way of feeding the working fluid to the different pressure levels and in the location of some heat exchangers. It is important to mention here that there are many more ways to combine the heat exchangers, which are not shown in Fig. 1 but included in the formulation of the model.

Insert Figure 1

In the process configuration shown in Fig. 1a, the three pressure levels are fed from the condenser. An LP economizer (section 10), an LP evaporator (section 9), and an LP superheater (section 8) are located in the coldest zone of the HRSG. Subsequently, in the intermediate-temperature zone, an MP economizer (section 7) and an MP evaporator (section 6) are located, followed by an HP economizer (section 5). Finally, in the hottest zone, an MP superheater, an HP evaporator, and a second MP superheater are placed, followed by an HP superheater (sections 4, 3, 2, and 1, respectively). In the process configuration shown in Fig. 1b, the LP and MP levels are fed from the condenser while the HP level is fed from the MP level. In this way, the HP economizer (section 5) is fed with a liquid stream with a temperature higher than that in Fig. 1a coming from the condenser, but implying a higher heat load in the MP economizer (section 8). On the other hand, the LP superheater – which was located in the section 8 in Fig. 1a – is now located in the section 7, where the gases can reach a higher temperature. Finally, in the process configuration shown in Fig. 1c, the MP and HP levels are fed from the corresponding inferior pressure level, i.e. the MP level from the LP level and the HP level from the MP level. This increases the temperature at which water enters the economizers but increases the heat load in the LP and MP levels (sections 9 and 7, respectively). Also, unlike in the previous two cases, an MP superheater is removed and only one heat exchanger is kept in the hottest gas section (section 1). In this configuration, the superheated steam stream coming from the steam turbines mixes with saturated steam and enters the unit of the section 1. In addition, the LP superheater is located in a zone hotter than in the previous configuration (Fig. 1b); indeed, it moves from the section 7 to 5.

In order to find the optimal configuration of the HRSG, the superstructure shown in Fig. 2 is proposed for optimization. As mentioned, this superstructure embeds, not only the process configurations shown in Fig. 1, but also many other candidate configurations, where the heat exchangers are combined in different alternative arrangements (as will be detailed in the presentation of the mathematical model).

Insert Figure 2

3. Optimization problem statement

Given are the process superstructure representation shown in Fig. 2 and the flow rate and inlet temperature of the flue gas stream. The optimization problem is formulated as follows.

Minimize (THTA)

subject to:

-Mass balances

-Energy balances

-Design equations (sizing)

-Thermodynamic property estimation equations

- Process design specifications (a fixed net electrical power generation).

As result, the optimal values of the following decisions are obtained:

- Discrete decisions:

  - Optimal structure (layout) of heat exchangers. This implies to select the number of the heat exchangers and their locations inside the HRSG indicating how they should be interconnected (series or series-parallel, or parallel arrangements).

  - Optimal number of pressure levels. The results should indicate if the HRSG should be operated with three or two or one pressure levels. For instance, if the high pressure level is removed, the associated economizer, evaporator and superheater must be also removed.

  - Optimal location of the reheating stream.

- Continuous decisions

  - Optimal allocation of the total heat transfer area.

  - Optimal values of mass flow rate, pressure, temperature, and composition of the process streams.

  - Optimal heat loads at the system components.

The proposed optimization problem is solved and compared with two reference cases taken from the literature. As will be shown in the next section, the main difference between the superstructure here proposed and the configurations of the reference cases is the possibility of using candidate pumps properly located to increase, if it is beneficial, the inlet pressure in the economizers. Another difference is the consideration of more candidate configurations of heat exchangers as well as different ways for steam reheating.

4. Mathematical model

The entire mathematical model consists of the mass and energy balances of each process unit (steam turbines, pumps, heat recovery steam generator), equations to calculate the associated heat transfer areas, installed power of turbines and pumps, and equations to estimate the physico-chemical properties of process streams. The main discrete decisions are those related to the configuration of the heat exchangers in the HRSG and the selection of the corresponding pumps. The configuration of the steam turbines is fixed but not their operating conditions and sizes. The main continuous decisions are the pressure, temperature, and flow rate of the process streams of each working fluid (gas in the gas turbine and water/steam in the steam turbines). Next, the main constraints used to model the discrete decisions associated with the HRSG are presented.

4.1 HRSG mathematical model

In order to perform an easier implementation of the model in GAMS and identification of each heat exchanger, the HRSG is divided into several sections and pressure levels, as shown in Fig. 3. To do this, the following sets are declared: the set 'I', with 13 elements 'i', is used to identify different sections of the HRSG and the set 'J', with 3 elements 'j', is used to identify the different pressure levels. Also, a set 'K', with 78 elements 'k', is declared to number the process streams associated with the *water/steam* working fluid. Thus, each heat exchanger is identified by a 3-tuple (i,j,k). As explained later, the element k is important to properly associate streams with heat exchangers. It should be noticed that the streams associated with the *gas* working fluid can be numbered using the set I already defined to identify the sections of the HRSG. Figure 3a shows the representation of a generic section i of the HRSG with a heat exchanger at each pressure level j (LP, MP, HP) with the used nomenclature, and Fig. 3b shows how it is instantiated for the section i=13. As illustrated, the three (candidate) heat exchangers located in the section i=13 are identified by the following 3-tuples (13,LP,1), (13,MP,13), and (13,HP,35). Now, an element k is linked to a specific heat exchanger, so it is convenient to define a subset HE that properly links elements k with elements i and j. That is, in Fig. 3b, the elements k=1, k=13, and k=35 correspond only to section i=13 and not to the rest of the sections. In this way, the subset HE contains all heat exchangers (31 heat exchangers) through the correspondence between i, j, and k. Finally, it is important to note that the evaporators are fixed in the superstructure and, therefore, no discrete decisions are associated with them. Then, a new subset EV is defined for evaporators in terms of set I. Thus, EV contains the three evaporators located in the sections i=3, 7, 11.

Insert Figure 3

4.1.1 Energy balances

Equation (1) calculates the heat load in a heat exchanger in the HRSG (in terms of the water/steam working fluid).

$$Q_{i,j} = m_{k+1}h_{k+1} - m_k h_k \qquad i,j,k \in HE(i,j,k) \tag{1}$$

Then, the energy balance in each section i is expressed as follows:

$$\sum_{j \in HE(i,j,k)} Q_{i,j} = m^G\left(h_i^G - h_{i+1}^G\right) \qquad \forall i \tag{2}$$

4.1.2 Heat transfer area

The heat transfer area $A_{i,j}$ required by the heat exchanger 'i,j,k' is calculated as follows:

$$Q_{i,j} = U_{i,j}A_{i,j}\Delta T_{i,j} \qquad i,j \in HE(i,j,k) \tag{3}$$

where $Q_{i,j}$, $U_{i,j}$, and $\Delta T_{i,j}$ refer to the heat load, the overall heat transfer coefficient, and the driving force, respectively.

The Chen approximation (Chen (1987) [49]) (Eq. (4)) is used instead of the logarithmic mean temperature difference (LMTD), because it facilitates the model convergence when a heat exchanger is removed from the superstructure.

$$\Delta T_{i,j} = \sqrt[3]{0.5\left(T_i^G - T_{k+1}\right)\left(T_{i+1}^G - T_k\right)\left[\left(T_i^G - T_{k+1}\right) + \left(T_{i+1}^G - T_k\right)\right]} \quad i,j,k \in HE(i,j,k) \tag{4}$$

4.2 Logical constraints to select economizers and superheaters

In order to select or remove a heat exchanger located in the section i at the pressure level j, the following two-term disjunction, expressed in terms of the Boolean variable $X_{i,j}$, is proposed:

$$\begin{bmatrix} X_{i,j} \\ Q_{i,j} \le \left|Q_{i,j}\right|_{up} \\ Q_{i,j} \ge \left|Q_{i,j}\right|_{lo} \end{bmatrix} \vee \begin{bmatrix} \neg X_{i,j} \\ Q_{i,j} = 0 \\ \ \end{bmatrix} \qquad i,j \in HE(i,j,k) \wedge i \notin EV(i) \qquad \text{(D1)}$$

The Boolean variable $X_{i,j}$ establishes whether a given term in the disjunction is TRUE or FALSE. The disjunction D1 states that, if $X_{i,j}$ is TRUE, then the optimal value of the variable $Q_{i,j}$ is lower than $\left|Q_{i,j}\right|_{up}$ (upper bound) and higher than $\left|Q_{i,j}\right|_{lo}$ (lower bound); consequently, $A_{i,j} \neq 0$ due to Eq. (3). Otherwise, if $X_{i,j}$ is FALSE, then $Q_{i,j} = 0$ and, consequently, $A_{i,j}$=0. The disjunction D1 does not apply for the subset EV (i=3, 7, 11) because it contains the three evaporators that are fixed in the superstructure. Then, by associating the binary variable $x_{i,j}$ with the Boolean variable $X_{i,j}$ and applying

Big-M reformulations, the proposed disjunction is translated into the following two algebraic inequality constraints:

$$Q_{i,j} \le x_{i,j} \left|Q_{i,j}\right|_{up} \qquad i,j \in HE(i,j,k) \wedge i \notin EV(i) \tag{5}$$

$$Q_{i,j} \ge x_{i,j} \left|Q_{i,j}\right|_{lo} \qquad i,j \in HE(i,j,k) \wedge i \notin EV(i) \tag{6}$$

As explained, if $x_{i,j} = 0$, then $Q_{i,j} = 0$ and, consequently, $A_{i,j} = 0$. Otherwise, if $x_{i,j} = 1$, then $Q_{i,j}$ is in between $\left|Q_{i,j}\right|_{lo}$ and $\left|Q_{i,j}\right|_{up}$ and, consequently, $A_{i,j} \neq 0$.

Disjunctions similar to D1 are proposed to select pumps and the location of the inlet of the steam stream for reheating, as described later.

4.2.1 Logical constraints to avoid equivalent solutions

Equivalent solutions can be frequently obtained when a superstructure-based model is proposed for optimization. That is, although the obtained values of the binary variables are different, it is possible to obtain optimal solutions that represent the same process configuration. Certainly, the superstructure proposed in Fig. 2 embeds several equivalent solutions when superheaters and/or economizers are removed from the superstructure.

Insert Figure 4

Figure 4 shows three equivalent solutions that may be obtained when only one low-pressure (LP) superheater is selected. It can be observed that the same resulting heat transfer process can be represented by selecting the superheater of either the section i=6 ($x_{6,LP}$=1, $x_{5,LP}$=0, $x_{4,LP}$=0 in Fig. 4a), or section i=5 ($x_{6,LP}$=0, $x_{5,LP}$=1, $x_{4,LP}$=0 in Fig. 4b), or section i=4 ($x_{6,LP}$=0, $x_{5,LP}$=0, $x_{4,LP}$=1 in Fig. 4c). Thus, the same values of heat transfer area, driving force, and amount of heat transferred between the streams #9 and #4 can be obtained by several combinations of the binary variables.

Other equivalent solutions can be obtained if two heat exchangers of the same type are selected. As shown in Fig. 5, in both configurations, the first heat exchange between the gas and water streams takes place at the MP level and the second one at the LP level. Thus, the same resulting configuration can be represented by two different sets of binary variable values ($x_{6,LP}$=1, $x_{5,MP}$=1, $x_{4,LP}$= $x_{4,MP}$ = $x_{4,HP}$=0 in Fig. 5a, and $x_{6,LP}$= $x_{6,MP}$= $x_{6,HP}$=0, $x_{5,LP}$=1, $x_{4,MP}$=1 in Fig. 5b).

Insert Figure 5

In order to avoid the occurrence of the equivalent solutions described in Figs. 4 and 5, it is proposed to select the heat exchangers from left to right, or equivalently, to remove them from right to left. To model this, the following logic propositions are imposed for two successive heat exchangers.

$$\neg\left(\bigvee_{j\in HE(i,j,k)} X_{i,j}\right) \Rightarrow \neg\left(\bigvee_{j\in HE(i-1,j,k)} X_{i-1,j}\right) \qquad i=13,10,9,6,5,2 \qquad \text{(D2)}$$

As presented, the logic propositions apply to the sections i=13, 10, 9, 6, 5, and 2, establishing that if no heat exchanger is selected in the section *i*, then no heat exchanger is selected in the previous section *i−1*. This logical proposition can be translated into the following algebraic inequality constraints (Eqs. (7)–(11)):

$$x_{i,LP} + x_{i,MP} + x_{i,HP} + 1 - x_{i-1,LP} \geq 1 \qquad i=13,10,9,6,5 \qquad (7)$$

$$x_{i,LP} + x_{i,MP} + x_{i,HP} + 1 - x_{i-1,MP} \geq 1 \qquad i=13,10,9,6,5 \qquad (8)$$

$$x_{i,LP} + x_{i,MP} + x_{i,HP} + 1 - x_{i-1,HP} \geq 1 \qquad i=13,10,9,6,5 \qquad (9)$$

According to Eqs. (7)–(9), if $x_{i,LP} = x_{i,MP} = x_{i,HP} = 0$, then $x_{i-1,LP} = x_{i-1,MP} = x_{i-1,HP} = 0$. Also, it can be observed that if $x_{i,LP} = 1$ or $x_{i,MP} = 1$ or $x_{i,HP} = 1$ or $x_{i,LP} = x_{i,MP} = x_{i,HP} = 1$, then $x_{i-1,LP}$, $x_{i-1,MP}$, and $x_{i-1,HP}$ can be individually 0 or 1. These three constraints apply to the sections that involve the three pressure levels. Since no low-pressure level is involved in the section i=2, the following constraints apply in this case:

$$x_{i,MP} + x_{i,HP} + 1 - x_{i-1,MP} \geq 1 \qquad i=2 \qquad (10)$$

$$x_{i,MP} + x_{i,HP} + 1 - x_{i-1,HP} \geq 1 \qquad i=2 \qquad (11)$$

However, it should be mentioned that no equivalent solutions can be obtained if three heat exchangers are selected, as illustrated in Fig. 6. In this case, the order in which the gas and water/steam streams exchange heat in Fig. 6a is different from that in Fig. 6b.

Insert Figure 6

4.2.2. Selection of the location and configuration of the reheating process

A similar disjunction to D1 is here proposed to select the steam stream that comes from the HP steam turbine ST1 for reheating. As shown in Fig. 2, the steam for reheating that comes from ST1 can be fed through five candidate streams (#53 to #57). The disjunction D3 is proposed in terms of the Boolean variable Z_k.

$$\begin{bmatrix} Z_k \\ m_k \leq \left|m_k\right|_{up} \\ m_k \geq \left|m_k\right|_{lo} \end{bmatrix} \vee \begin{bmatrix} \neg Z_k \\ m_k = 0 \\ \end{bmatrix} \qquad 53 \leq k \leq 57 \qquad \text{(D3)}$$

As established in D3, if Z_k is TRUE, then the optimal value of the variable m_k is lower than $\left|m_k\right|_{up}$ (upper bound) and higher than $\left|m_k\right|_{lo}$ (lower bound); consequently, $m_k \neq 0$. Otherwise, if Z_k is FALSE, then $m_k = 0$. Then, by associating the binary variable z_k with the Boolean variable Z_k, D3 is translated into the following two algebraic inequality constraints:

$$m_k \le z_k \left|m_k\right|_{up} \qquad 53 \le k \le 57 \tag{12}$$

$$m_k \ge z_k \left|m_k\right|_{lo} \qquad 53 \le k \le 57 \tag{13}$$

As a first approximation, only one of these candidate streams can be selected, what is imposed through the logical proposition D4, which leads to the algebraic constraint given by Eq. (14):

$$Z_{53} \veebar Z_{54} \veebar Z_{55} \veebar Z_{56} \veebar Z_{57} \tag{D4}$$

$$\sum_{k=53}^{57} z_k = 1 \tag{14}$$

4.2.3 Selection of the working fluid pumps

A similar disjunction to D1 is also proposed to select the required pumps (D5). As shown, a pump is selected in terms of the associated flowrate value. If a pump is not selected, then the associated inlet flow is zero.

$$\begin{bmatrix} Y_n \\ m_k \le \left|m_k\right|_{up} \\ m_k \ge \left|m_k\right|_{lo} \end{bmatrix} \vee \begin{bmatrix} \neg Y_n \\ m_k = 0 \\ \end{bmatrix} \qquad n,k \in PUMP(n,k,k') \wedge n \le 9 \tag{D5}$$

Then, by associating the binary variable y_k with the Boolean variable Y_n, D5 is translated into the following two algebraic inequality constraints:

$$m_k \le y_n \left|m_k\right|_{up} \qquad n,k \in PUMP(n,k,k') \wedge n \le 9 \tag{15}$$

$$m_k \ge y_n \left|m_k\right|_{lo} \qquad n,k \in PUMP(n,k,k') \wedge n \le 9 \tag{16}$$

For instance, in Fig. 2, if the value of the binary variable associated to the pump #9 (y_9) is zero, then Eqs. (15) and (16) force the associated flow to be zero ($m_{77} = 0$), which is equivalent to eliminating the pump from the solution.

On the other hand, the feed inlet to the MP and HP levels may optionally come from the condenser or from an inferior pressure level (i.e. MP from LP and HP from MP), as is shown in Fig. 2.

Propositions D6 and D7 are included in the model in order to select a unique feed pump at the MP and HP levels, which lead to the algebraic constraints given by Eqs. (17) and (18):

$$Y_1 \veebar Y_2 \veebar Y_9 \tag{D6}$$

$$Y_3 \veebar Y_4 \veebar Y_5 \veebar Y_6 \veebar Y_7 \veebar Y_8 \tag{D7}$$

$$y_1 + y_2 + y_9 = 1 \tag{17}$$

$$y_3 + y_4 + y_5 + y_6 + y_7 + y_8 = 1 \tag{18}$$

4.2.4 Logical constraints between heat exchangers and pumps

It is interesting to note that there are also logical relationships between candidate heat exchangers and candidate pumps that may lead to equivalent solutions when deciding the presence (or absence) of pumps by solving the proposed superstructure-based optimization model. To avoid the occurrence of these equivalent solutions, the following two considerations are made.

Consideration 1: if there is no economizer feeding the pump, then the pump does not exist (proposition D8). The Boolean variable Y_n represents the existence of the pump ‘n’. The subset NHNP relates the economizer ‘(i,j)’ to the pump ‘n’.

$$\neg X_{i,j} \Rightarrow \neg Y_n \quad \forall i,j,n \in NHNP(i,j,n) \tag{D8}$$

Then, the logical proposition D8 is translated into the algebraic constraint given by Eq. (19):

$$x_{i,j} + 1 - y_n \geq 1 \qquad \forall i,j,n \in NHNP(i,j,n) \tag{19}$$

Consideration 2: if a certain economizer exists, then there are no pumps after it at the inferior pressure level (proposition D9). The HNP subset relates the exchanger ‘(i,j)’ to the pump ‘n’.

$$X_{i,j} \Rightarrow \neg Y_n \qquad \forall i,j,n \in HNP(i,j,n) \tag{D9}$$

The logical proposition D9 is translated into the algebraic constraint given by Eq. (20):

$$1 - x_{i,j} + 1 - y_n \geq 1 \qquad \forall i,j,n \in HNP(i,j,n) \tag{20}$$

In this way, Eqs. (15)–(20) allow an orderly elimination by relating the heat exchangers and the associated pumps as appropriate.

4.2.5 Possibility of selecting parallel heat exchangers

As mentioned earlier, the HRSG superstructure also includes the possibility of selecting heat exchangers operating in parallel at each section of the HRSG, except for the sections that contain evaporators. This possibility is allowed by the following constraint:

$$\sum_{j \in HE(i,j,k)} x_{i,j} \leq PE_i \qquad i \notin EV(i) \tag{21}$$

where PE_i refers to the maximum number of heat exchangers operating in parallel at the section i; it is a model parameter that can be varied.

4.2.6 Possibility of limiting the number of economizers and superhetars at each pressure level

In addition, the model includes constraints related to the maximum number of economizers EC_j (Eq. (22)) and superheaters SH_j (Eq. (23)) that are allowed to operate at each pressure level j (LP, MP, and HP):

$$\sum_{i \in EC(i,j)} x_{i,j} \leq EC_j \qquad \forall j \tag{22}$$

$$\sum_{i \in SH(i,j)} x_{i,j} \leq SH_j \qquad \forall j \tag{23}$$

EC_j and SH_j are model parameters that can be varied.

4.3 Calculation of the physical-chemical properties

The use of dynamic-link libraries (DLLs) as well as extrinsic functions allows to significantly enhance the model implementation compared to the traditional approach, and to considerably reduce the model size as well as the computational time required by the optimization algorithms. For instance, a MINLP model to optimize the process configuration of two coupled distillation columns including DLLs and extrinsic functions required almost 4000 constraints and variables less than if no DLLs and extrinsic functions are employed (Manassaldi et al. 2019). In addition, the time required to solve the NLP models was less than half in comparison with models without employing DLLs and extrinsic functions.

4.4 Objective function

The optimization criterion is the minimization of the total heat transfer area (THTA) which is calculated in Eq. (24):

$$THTA = \sum_{i,j \in HE(i,j,k)} A_{i,j} + A_{COND} \tag{24}$$

where A_{COND} refers to the heat transfer area of the condenser in the Rankine cycle.

5. Discussion of results

The results discussed in this section correspond to the performed model verification and the obtained optimal solutions.

Tables 1 and 2 list the numerical values of the model parameters and the lower and upper bounds, respectively, used for all optimizations.

Table 1. Values of model parameters used in all case studies.

Flue gas specification			Source
Mass flow rate of gas turbine exhaust gases	kg/s	445.4	(Franco and Giannini, 2006)
Temperature of gas turbine exhaust gases	K	778.15	(Franco and Giannini, 2006)
Minimum outlet temperature of gases leaving HRSG	K	348.15	(Franco and Giannini, 2006)
Process units			
Economizer overall heat transfer coefficient	W/(m^2 K)	42.60	(Franco and Russo, 2002)
Evaporator overall heat transfer coefficient	W/(m^2 K)	43.70	(Franco and Russo, 2002)
Superheater overall heat transfer coefficient	W/(m^2 K)	50.00	(Franco and Russo, 2002)
Minimum pinch point	K	10.00	(Franco and Giannini, 2006)
Minimum heat transfer temperature difference	K	10.00	(Franco and Giannini, 2006)
Condenser pressure	bar	0.1733	(Franco and Giannini, 2006)
Isentropic efficiency of steam turbines	dimensionless	0.90	(Franco and Russo, 2002)
Efficiency of pumps	dimensionless	0.75	(Manassaldi et al., 2016)

Table 2. Lower and upper bounds on optimization variables used in all case studies.

Variable		Lower bound	Upper bound
High pressure (P^{HP})	bar	110	180*
Medium pressure (P^{MP})	bar	10	60
Low pressure (P^{LP})	bar	1	10
Temperature (T)	K	330.15*	768.15*
Mass flow rate (m)	kg/s	0	100

* Value taken from Franco and Giannini (2006).

The proposed mathematical model involves 588 continuous variables, 42 binary variables, and 773 constraints (equality and inequality constraints) and was implemented in GAMS 23.9.5 (General Algebraic Modeling System). SBB (Standard Branch and Bound) (Bussieck and Drud, 2001) and CONOPT (Drud, 1992) are the solvers used for the mixed-integer nonlinear problems (MINLP) and nonlinear problems (NLP), respectively. SBB is employed because it is suitable for solving models that have fewer discrete decisions but more difficult nonlinearities (https://www.gams.com/latest/docs/S_SBB.html#SBB_COMPARISON_OF_DICOT_AND_SBB), characteristics involved by the model proposed in this work.

In the current model, DLLs are used to calculate the enthalpy, entropy, specific volume, and density of the working fluid of the steam cycle (water, steam). As shown in Fig. 7, extrinsic functions associated to the correlations reported in 'Revised Release on the IAPWS Industrial Formulation 1997 for the Thermodynamic Properties of Water and Steam' (IAPWS R7-97, 2012) are declared in the C programming language in a DevC++ project generating the corresponding DLLs (extrinsic.DLL), which are included in GAMS ($funclibin IAPWS iapws.dll) and executed outside GAMS.

Insert Figure 7

In the file *extrfunc.h* all the definitions required to create the libraries are included. In the file *mylibraryql.c* the architectures of the library and the functions are defined. Finally, in the *mylibrary.c* the functions are programmed and/or imported. As illustrated in Fig. 7, for each physicochemical property an extrinsic function has been declared. A detailed description about the implementation of DLLs for all physicochemical properties and how they interact with GAMS can be found in Manassaldi et al. (2019). The IAPWS.dll library is available and can be downloaded from the GAMS World Forum (https://forum.gamsworld.org/viewtopic.php?f=16&t=11547). The model involves many nonlinear constraints. For instance, the domains of many functions from the IAPWS-IF97 are nonconvex (Bongartz et al., 2020). Also, bilinear terms appearing in the energy balances as well as in the design equations used to calculate the heat transfer areas of all heat exchangers are involved.

5.1 Model verification

The proposed model was successfully verified by comparing the model output with the optimal solution presented in Franco and Giannini (2006) , whose optimal process configuration – hereafter referred as the 'RC configuration' – is illustrated in Fig. 8. In order to perform a correct verification and because the MINLP model developed in this work embeds many candidate configurations, several (discrete and continuous) model variables were fixed at the optimal values reported for the RC configuration. Then, an optimization problem consisting in the minimization of the sum of the square errors between the data taken from Franco and Giannini (2006) and the values calculated by the model (Eq. (25)), was solved:

$$Min\left(\sum_{k\in MK(k)}\left(m_k^{FG}-m_k\right)^2+\sum_{k\in PK(k)}\left(P_k^{FG}-P_k\right)^2+\sum_{k\in TK(k)}\left(T_k^{FG}-T_k\right)^2+\sum_{(i,j)\in QK(i,j)}\left(Q_{i,j}^{FG}-Q_{i,j}\right)^2\right) \quad (25)$$

where the subscript FG refers to data reported by Franco and Giannini (2006); the subsets *MK*, *PK*, *TK* contain the stream k with mass flow rate m_k, pressure P_k, temperature T_k, respectively. The subset *QK* contains the heat load Q of the heat exchanger *i,j*.

Table 3 compares the values of pressure, temperature, and mass flow rate of the streams of the circulating fluid in the Rankine cycle. Table 4 compares the gas stream temperatures. Table 5 compares the values of the total heat load in the HRSG and in each heat exchanger. The values that were fixed in the MINLP model and that are used in Eq. (25) are marked with the symbol * in these tables. The remaining variables listed in the tables are the outputs used for comparison. The three tables include the percentage error computed for each variable.

Insert Figure 8

Table 3. Comparison of the pressure, temperature, and mass flow rate values of the streams of the circulating fluid in the Rankine cycle reported by Franco and Giannini (2006) and the obtained in this work (MINLP model).

Stream # of the working fluid in the Rankine cycle	Franco and Giannini (2006)			This work			Error (%)		
	P (bar)	T (K)	m (kg/s)	P (bar)	T (K)	m (kg/s)	P (bar)	T (K)	m (kg/s)
6	6.0	432.0	13.62	6.0*	432.0	13.62*	0.00%	0.02%	0.00%
12	6.0	501.1	13.62	6.0	501.1*	13.62*	0.00%	0.00%	0.00%
18	53.0	501.1	45.79	54.387	501.1*	45.801	−2.62%	0.00%	−0.02%
24	53.0	540.7	15.33	54.387	542.4	15.353	−2.62%	−0.31%	−0.15%
26	53.0	603.1	15.33	54.387	603.4	15.353	−2.62%	−0.05%	−0.15%
28	53.0	624.9	45.79	54.387	624.9	45.801	−2.62%	0.00%	−0.02%
34	53.0	768.1	45.79	54.387	768.1	45.801	−2.62%	0.00%	−0.02%
49	169.0	624.9	30.46	168.525	624.7	30.449	0.28%	0.04%	0.04%
51	169.0	768.1	30.46	168.525	768.1*	30.449	0.28%	0.00%	0.04%
75	0.1733	330.1	59.41	0.1733*	330.1*	59.421	0.00%	0.00%	−0.02%

* Numerical values fixed in the MINLP model that are used in Eq. (25).

Table 4. Comparison of the temperature values of the gas streams reported by Franco and Giannini (2006) and the obtained in this work (MINLP model).

	T^G (K)		
Stream # of gas	Franco and Giannini (2006)	This work	Error (%)
1	778.1	778.1 *	0.00%
3	702.6	704.4	-0.26%
4	651.1	652.7	-0.24%
6	634.9	636.7	-0.27%
7	607.8	610.0	-0.36%
8	558.1	560.7	-0.46%
10	540.8	542.3	-0.27%
11	508.3	509.5	-0.23%
12	450.3	451.5	-0.26%
14	395.6	398.5	-0.72%

* Numerical value fixed in the MINLP model that are used in Eq. (25).

Table 5. Comparison of the values of the total heat load in the HRSG and in each heat exchanger reported by Franco and Giannini (2006) and the obtained in this work (MINLP model).

	Heat load (MW)		
	Franco and Giannini (2006)	This work	Error (%)
Total	**191.43**	**190.23**	**0.63**
Heat exchanger (i,j)			
(13,LP)	26.24	25.63	−2.36
(10,MP)	14.14	14.11	−0.21
(9,MP)	8.59	9.15	6.16
(6,HP)	10.5	10.19	−3.04
(5,HP)	5.09	5.19	2.00
(11,LP)	28.39	28.41	0.06
(7,MP)	24.86	24.70	−0.64
(3,HP)	26.29	26.45	0.60
(10,LP)	1.95	2.11	7.61
(6,MP)	3.16	3.26	3.11
(5,MP)	3.12	2.93	−6.57
(2,MP)	17.24	16.23	−6.20
(2,HP)	21.86	21.86	−0.01

According to the values listed in Tables 3 and 4, the maximum deviation is −2.62%, which corresponds to the pressure of stream #18. This deviation may be due to the fact that the correlations used by Franco and Giannini (2006) to estimate the enthalpy and vapor pressure values of the circulating fluid at different conditions (superheated and saturated steam, subcooled and saturated liquid) are different from those used in this study. The deviations in the rest of the variables are practically insignificant. Regarding the deviations computed for heat loads, it can be seen in Table 5 that the deviation in the total heat load in the HRSG is only 0.63% (191.43 MW vs. 190.23 MW), with the particularity that the calculated values for some heat exchangers are higher than those reported by Franco and Giannini (2006) , but for others they are lower. However, the variations along the HRSG compensate, resulting in a total deviation of 0.63%. Then, based on the obtained percentage deviations, it can be concluded that, for the purpose of this study, the implemented process model successfully predicts the solution reported by Franco and Giannini (2006).

5.2 Optimization results

This section presents the optimization results obtained by solving the problem stated in Section 3, which consists in determining the optimal configuration of the heat exchangers with their corresponding sizes and operating conditions that minimize the total heat transfer area of the HRSG to generate a fixed, specified total net power. For comparison purpose, it is specified the total net power value calculated in Franco and Giannini (2006) (RC configuration), which is equal to 63.026 MW. The obtained optimal solution is hereafter named 'OS'.

Insert Figure 9

For all optimization cases, the numerical values of the model parameters and bounds on decision variables are the same as those listed in Tables 1 and 2. In addition, the model has been solved by setting the option *optcr* at the minimum value supported by the solver ($1.0x10^{-9}$). To obtain the integer solution of this case study, the optimization algorithm explored 34 nodes and stopped with a relative gap of $9.34x10^{-16}$ requiring 3773 iterations and 23.32 NLP seconds.

Figure 9 illustrates the optimal configuration corresponding to OS and Fig. 10 compares the T-H diagrams resulting from the RC and OS solutions. Tables 6–10 compare the optimal values obtained for both RC and OS solutions.

Table 6. Comparison of optimal values obtained for RC and OS solutions (gas temperature, total heat load, and total heat transfer area in each HRSG zone).

		Gas temperature (K)		Heat load (MW)		Heat transfer area ($x10^3$ m^2)	
Point	HRSG zone	RC	OS	RC	OS	RC	OS
1		778.1	778.1	64.54	**68.57**		
2	Hot zone	778.1	745.8	(3 HEXs)	(5 HEXs)		
3		704.5	710.0	2,HP/2,MP/3,HP	1,HP/1,MP/2,HP	35.40	**25.65**
4		652.7	644.7		2,MP/3,HP		
5		652.7	642.7	46.27	**62.25**		
6		636.7	578.2	(5 HEXs)	(6 HEXs)		
7	Intermediate	610.0	572.8	5,HP/5,MP/6,HP/	4,MP/5,HP/5,MP/		
8	zone	560.7	520.4	6,MP/7,MP	6,MP/6,LP/7,MP	27.17	**30.36**
9		560.7	520.4				
10		542.3	520.4	79.41	**61.31**		
11		509.5	482.7	(5 HEXs)	(7 HEXs)		
12	Cold zone	451.5	438.2	9,MP/10,MP/	10,HP/10,MP/10,LP		
13		451.5	438.2	10.LP/11,LP/13,LP	11,LP/13,HP/	45.13	**35.72**
14		398.6	394.5		13,MP/ 13,LP		
				190.23	**192.14**	**107.70**	**91.74**

Figures 8 and 9 clearly show the differences that exist between the configuration reported by Franco and Giannini (2006) (RC) and the optimal configuration obtained by the proposed model (OS). As can be seen in Fig. 9, the optimal number of heat exchangers in OS is 18, i.e., 5 heat exchangers more than in RC (Fig. (8)). According to the results listed in Tables 6 and 7, it can be observed that the total heat exchanged between the gas and the circulating fluid in the hottest zone of the HRSG (sections i =1–3) is similar (64.54 MW in RC vs. 68.57 MW in OS) because the difference in the gas outlet temperature in this zone (i = 3) – which is an optimization variable of the model – only differs in 8 K (652.7 K in RC vs. 644.7 K in OS, Table 6). While the gas inlet temperature and flow rate in the section i = 1 are the same in both configurations since, as mentioned above, they are fixed and known values – i.e. model parameters – taken from Franco and Giannini (2006). Although in the hot zone the total heat exchanged in OS is slightly higher than in RC (4.03 MW according to Table 7), the area required in OS is 27.54 % lower than that required in RC (25650 m^2 vs. 35400 m^2), which is obtained using 2 heat exchangers more than in RC, specifically two superheaters (1,HP) and (1,MP) at the high and medium pressure levels, respectively. In the OS configuration (Fig. 9), in addition to the evaporator EV1 (i = 3), sections i = 1 and 2 involve 4 heat exchangers in total, with 2 exchangers in each section, where the gas stream exchanges heat in parallel with the circulating fluid at MP and HP levels. On the other hand, in the RC configuration (Fig. 8), there are only 2 parallel heat exchangers, precisely in the section i = 2. The fact of using 4 heat exchangers in OS – not 2 as in RC – allows to increase the degrees of freedom of the optimization problem since it is possible to conveniently vary, not only the temperature of both the gas stream and circulating fluid, but also the corresponding flow rates, in such a way that the heat transfer area in OS is smaller than in RC to transfer practically the same amount of total heat in this zone of the HRSG. According to the values listed in Table 7 for OS, the heat exchangers selected in the MP and HP levels in the section i = 2 ((2,MP) and (2,HP)) require 1530 m^2 and 3000 m^2, respectively, to transfer 6.11 MW and 12.37 MW, with a driving force of 80.04 K and 82.47 K, respectively. While for RC, Table 7 shows that these two heat exchangers require 9870 m^2 and 13260 m^2 to transfer 16.23 MW and 21.86 MW, respectively, with a driving force of 32.90 K and 32.95 K. In the section i = 1, the heat exchangers (1,MP) and (1,HP) selected in OS require 3270 m^2 and 3950 m^2, respectively, to transfer 7.71 MW and 9.04 MW with a driving force of 47.17 K and 45.81 K. The section i = 3 involves the evaporator (3,HP), which is fixed in the superstructure i.e. it is not a decision variable, as mentioned in the model presentation. The heat transfer area required by (3,HP) in OS is 1630 m^2 larger than in RC, transferring 6.87 MW more than in RC (33.32 MW vs. 26.45 MW) with a driving force 5.51 K greater (54.84 K in OS vs. 49.33 K in RC). The operating temperature in (3,HP) – which corresponds to stream #49 of saturated steam in Table 8 – in OS is 8.65 K lower than in RC (616.08 K vs. 624.73 K) and the associated flow rate in OS is 3.185 kg/s higher (33.634 kg/s vs. 30.449 kg/s). The temperature-enthalpy (T-H) diagrams corresponding to both RC and OS configurations are compared in Figure 10, which allow visualizing how these variables are influenced by the inclusion of 2 parallel heat exchangers in the section i = 1, affecting significantly the driving forces and the heat transfer areas of the different process units.

In the intermediate-temperature zone of the HRSG, consisting of sections i = 4–8, in addition to the evaporator EV2 (i=7), the OS configuration includes one heat exchanger more than the RC configuration (5 vs. 4) and it shows a different arrangement of the process units and a different location of the inlet point of the stream associated with the reheating of the steam coming from the turbine ST1. Unlike in the hot zone, the gas outlet temperature in the intermediate zone (T_9 in Table 6) is 520.4 K in OS and 560.7 K in RC, resulting in a recovered heat amount and a heat transfer area required in OS by around 34.53% and 11.74% higher than in RC, respectively (62.25 MW vs. 46.27 MW and 30360 m^2 vs. 27170 m^2, according to Table 7). By comparing Figs. 8 and 9 it can be seen that the heat exchanged in parallel between the gas stream and the circulating fluid in the section i = 6 takes place at LP and MP levels in OS (i.e. in (6,LP) and (6,MP)); whereas in RC the heat exchanges take place at MP and HP levels (i.e. in (6,MP) and (6,HP)). Another difference is the location at which steam superheating begins. In the OS configuration (Fig. 9), the steam leaving the turbine ST1 mixes with the saturated steam leaving the evaporator (7,MP) (stream #25) and enters the superheater (6,MP). Differently, in RC (Fig. 8), the stream leaving the evaporator (7,MP) is first reheated in the superheater (6,MP) and then it is mixed with the stream leaving ST1 (stream #25), entering a second superheater (5,MP). The T-H diagrams (Fig. 10) show the temperature differences on the hot and cold sides of each heat exchanger of both configurations, which determine the corresponding driving forces that affect the heat transfer areas. Compared to RC, Fig. 10 and Tables 7 and 8 show that the operating temperature in the evaporator (7,MP) in OS is 45.3 K lower (497.13 K vs. 542.40 K, in Table 8), its heat load is slightly higher (26.06 MW vs. 24.70 MW, in Table 7) but requiring less heat transfer area (13450 m^2 vs. 15030 m^2, in Table 7) as a result of the temperature differences at the ends of the evaporator (23.3 K vs. 18.3 K at the cold end and 75.7 K vs 67.6 K at the hot end), which implies a greater driving force (44.3 K vs. 37.6 K, in Table 7). The heat exchanger (6,MP) exhibits a different behavior to that observed for (7,MP) since the heat load in OS is 1.17 MW lower than in RC (2.09 MW vs. 3.26 MW), requiring less heat transfer area (680 m^2 vs. 1350 m^2) with a driving force of 61.1 K, which is 12.76 K greater than in RC (48.4 K). However, the heat exchangers (5,HP) and (5,MP) exhibit a different behavior from the previous ones (7,MP and 6,MP) since not only the heat loads but also the heat transfer areas in OS are greater than those in RC, although the associated driving forces in OS are still greater than in RC. Precisely, the heat transfer areas required in OS by (5,HP) and (5,MP) are 10510 m^2 and 4830 m^2, respectively, while those required in RC are 3970 m^2 and 1890 m^2, respectively. From the analysis performed for each section of the intermediate-temperature zone of the HRSG, it is concluded that the transfer area increases of the heat exchangers (6,LP), (5,HP), and (5,MP) prevail over those of the heat exchangers (7,MP), (6,HP), and (6,MP), implying an increase of the total heat transfer area in OS with respect to RC (30360 m^2 vs. 27170 m^2).

Table 7. Comparison of solutions obtained for RC and OS configurations (heat load, driving force, and heat transfer area values for each heat exchanger and HRSG zone).

Heat exchanger ('section'.'pressure level')	HRSG zone	RC solution			OS solution		
		Q (MW)	DF (K)	Area (x10^3 m^2)	Q (MW)	DF (K)	Area (x10^3 m^2)
1,MP		0	10	0	7.71	47.17	3.27
1,HP		0	10	0	9.04	45.81	3.95
2,MP	Hot zone	16.23	32.90	9.87	6.11	80.04	1.53
2,HP		21.86	32.95	13.26	12.37	82.47	3.00
3,HP		26.45	49.33	12.27	33.32	54.84	13.90
Total		**64.54**	**-**	**35.40**	**68.57**	**-**	**25.65**
4,MP		-	27.73	-	1.01	29.01	0.70
5,HP		5.19	30.65	3.97	22.00	49.12	10.51
5,MP		2.93	30.95	1.89	10.51	43.54	4.83
6,HP		10.19	48.58	4.92	0	79.20	0
6,LP	Intermediate zone	0	121.71	0	0.58	62.18	0.19
6,MP		3.26	48.39	1.35	2.09	61.15	0.68
7,MP		24.70	37.62	15.03	26.06	44.34	13.45
Total		**46.27**	**-**	**27.17**	**62.25**	**-**	**30.36**
9,MP		9.15	28.20	7.62	0	23.26	0
10,HP		0	195.31	0	11.70	41.54	6.61
10,LP		2.11	57.43	0.735	1.79	39.50	0.91
10,MP		14.11	57.43	5.77	5.05	40.95	2.90
11,LP	Cold zone	28.41	41.88	15.52	21.68	39.29	12.63
13,LP		25.63	38.85	15.49	3.73	38.82	2.25
13,MP		0	92.32	0	5.17	39.11	3.10
13,HP		0	92.32	0	12.19	39.07	7.32
Total		**79.41**	**-**	**45.13**	**61.31**	**-**	**35.72**
Condenser		126.31	14.36	2.58	128.83	14.36	2.64
Total		**316.54**	**-**	**110.29**	**320.97**	**-**	**94.37**

Finally, when comparing the cold zone of the HRSG (sections i = 9–13) between the RC and OS configurations (Figs. 8 and 9, respectively), it can be seen that both the number of heat exchangers and their configurations, as well as the amount of transferred heat and required transfer area, are different. Precisely, the OS and RC configurations require 7 and 5 heat exchangers, respectively, to transfer in total 61.31 MW and 79.41 MW, with a total area of 35720 m^2 and 45130 m^2 in each case (Tables 6 and 7). It is important to note that, although the temperature of the gas stream leaving the cold zone (section i = 13, stream #14) in OS is 4.1 K lower than in RC (394.5 vs. 398.6 K), the inlet temperature is 40.3 K lower (520.4 K vs. 560.7 K), resulting in a lower total heat load (Table 6). Except for the section i = 11, which consists of an evaporator in both configurations, Fig. 9 shows that the remaining sections (i = 10, 13) are composed of 3 heat exchangers, in which the gas stream exchanges heat in parallel with each of the circulating fluids at the three pressure levels (3 economizers in the section i = 13 and 2 economizers and 1 reheater in the section i = 10), unlike what is observed in Fig. 8 for RC, where only 1 heat exchanger is present in the section i = 13 (economizer) and 2 heat exchangers in the section i = 10 (economizer and reheater). Figure 9 clearly shows that the circulating fluid stream splits and enters the section i = 1 in OS at the three pressure levels (LP, MP, and HP), unlike what happens in RC (Fig. 8), where the circulating fluid stream enters the section i = 1 at the LP level only (stream #1). As indicated in Fig. 8 for RC, once the stream #1 is preheated in the economizer (13,LP), it is divided into the stream #3, which enters the evaporator (11,LP), and stream #58, which starts circulating at the MP level by the pump P1 that is selected from the model. Afterward, the stream #20 leaving the economizer (9,MP) is divided into the stream #21, which enters the evaporator (7,MP), and stream #65, which starts circulating at the HP level by the pump P6.

The T-H diagrams (Fig. 10) allow to see how the temperatures of the circulating fluids (water/steam) corresponding to the three pressure levels and the temperatures of the gas stream are distributed along the HRGS to transfer the amount of heat needed in each piece of equipment, in order to satisfy the total energy balance and obtain the necessary driving forces for a minimal total heat transfer area. Comparing the trends shown by the process units that are present in both configurations – (13,LP), (11,LP), (10,MP), and (10,LP) –, it can be concluded that, except for exchanger (10,LP), all of them have a heat load and an associated transfer area in RC greater than in OS. Differently, the heat exchanger (10,LP) presents the highest heat load but the lowest heat transfer area.

As a summary of the analysis performed in each zone of the HRSG, it can be concluded that, although the total heat loads of the HRSG corresponding to both the RC and OS configurations are very similar (190.23 MW and 192.14 MW, respectively), the total heat transfer area required in OS is 14.82% lower than in RC (91740 m^2 vs. 107700 m^2). This is due to the inclusion in OS of 4 heat exchangers more than in RC, making it possible to modify the RC configuration, include parallel exchanges along the HRSG, and obtain more appropriate driving forces (temperature differences at the cold and hot sides) in each heat exchanger. Compared to the RC solution, the heat transfer area in the hot and cold zones of the HRSG required in the OS solution is 19160 m^2 smaller, but it is 3190 m^2 larger in the intermediate-temperature zone, resulting in a net reduction of 15970 m^2 in the HRSG. The results listed in Table 7 corresponding to the condenser indicate that the OS solution requires transferring 128.83 MW with an area of 2640 m^2, compared with 126.31 MW and 2580 m^2, respectively, required in the RC solution.

Insert Figure 10

Table 8. Comparison of the operating conditions in RC and OS configurations.

	RC			OS		
water stream	P (bar)	T (K)	m (kg/s)	P (bar)	T (K)	m (kg/s)
1	6.0	330.15	59.421	4.024	330.15	10.166
5	6.0	431.98	13.620	4.024	416.98	10.166
6	6.0	431.98	13.620	4.024	416.98	10.166
7	6.0	501.15	13.620	4.024	498.87	10.166
12	6.0	501.15	13.620	4.024	526.46	10.166
14	54.387	330.15	0	25.01	416.60	14.166
18	54.387	501.15	45.801	25.01	497.13	14.166
23	54.387	542.40	15.353	25.01	497.13	14.166
24	54.387	542.40	15.353	25.01	497.13	14.166
25	54.387	542.40	15.353	25.01	506.78	47.80
26	54.387	603.44	15.353	25.01	521.70	47.80
27	54.387	602.27	45.801	25.01	521.70	47.80
28	54.387	624.95	45.801	25.01	609.98	47.80
31	54.387	624.95	45.801	25.01	619.16	47.80
32	54.387	768.15	45.801	25.01	675.74	47.80
34	54.387	768.15	45.801	25.01	748.23	47.80
36	168.525	330.15	0	151.451	416.66	33.634
40	168.525	330.15	0	151.451	496.29	33.634
46	168.525	603.15	30.449	151.451	496.29	33.634
48	168.525	624.73	30.449	151.451	616.08	33.634
49	168.525	624.73	30.449	151.451	616.08	33.634
50	168.525	768.15	30.449	151.451	673.88	33.634
51	168.525	768.15	30.449	151.451	751.16	33.634
52	54.387	601.68	30.449	25.01	511.11	33.634
72	6.0	489.65	45.801	4.024	516.79	47.80
73	6.0	492.27	59.421	4.024	518.49	57.966
74*	0.1733	330.15	59.421	0.1733	330.15	57.966
75	0.1733	330.15	59.421	0.1733	330.15	57.966

* Stream with steam quality: 0.8988 in RC and 0.9398 in OS.

Finally, Table 9 compares the power generation in each steam turbine and the power consumption in each pump obtained in both solutions. As can be seen, the net power generation in both solutions is 63.026 MW, which is obtained in OS by producing 63.768 MW in the three steam turbines (ST1, ST2, and ST3) since an amount of 0.742 MW is required to operate the pumps P8, P9, and P10. While an amount of 64.001 MW is generated in RC, since the total consumption of the three pumps (P1, P6, and P10) is 0.975 MW.

Insert Figure 11

Table 9. Comparison of the electric power generated and required in RC and OS configurations.

	W [MW]	
Turbine	RC (Franco and Giannini, 2006)	OS (This work)
HP steam turbine (ST1)	8.307	13.364
MP steam turbine (ST2)	24.329	21.784
LP steam turbine (ST3)	31.365	28.619
Total	64.001	63.768
Pump		
P1	0.325	0
P2	0	0
P3	0	0
P4	0	0
P5	0	0
P6	0.603	0
P7	0	0
P8	0	0.689
P9	0	0.048
P10	0.047	0.005
Total	0.975	0.742
Net electric power	63.026	63.026

Figure 11 illustrates the contribution of each steam turbine to the total power generation. In both solutions, the largest fraction of the generated power is produced by the LP steam turbine (ST3) and the lowest fraction by the HP steam turbine (ST1). Also, it can be seen that the HP steam turbine generates more power in OS than in RC, contrary to what happens with the MP and LP steam turbines.

Table 10 summarizes the main differences between the RC and OS solutions.

Table 10. Main optimal (discrete and continuous) values associated with the synthesis and design of the HRSG obtained in the RC and OS solutions.

	RC	OS
Total number of heat exchangers	13	18
Economizers	5	6
Evaporators	3	3
Superheaters	5	9
Number of sections with parallel heat exchangers	4	6
Number of inlet streams of the working fluid	1	3
Number of pumps	3	3
Location of the steam leaving turbine ST1 for reheating	After the first superheater in the MP level	After the evaporator in the MP level
Total flow rate of the working fluid (kg/s)	59.421	57.966
Total heat recovered in HRSG (MW)	190.23	192.14
Total heat transfer area required in HRSG (x10^3 m^2)	110290	94370
Total power generated in steam turbines (MW)	64.00	63.77
Total power required by pumps (MW)	0.975	0.742

5.4 Comparison of results considering an existing CCPP.

The proposed model was solved considering data reported in Almutairi et al. (2015) corresponding to a single block of the Sabiya CCPP, in Kuwait, which includes a 3P HRSG with 14 heat exchangers arranged in series. Given the total electric power generated by the steam turbines – 125.39 MW per HRSG i.e. 250.78 MW in total with two HRSGs – and the heat load – 351.69 MW required in each HRSG, the optimization problem consisted in finding the optimal HRSG configuration and operating conditions that minimize the total heat transfer area. The model is solved by allowing an economizer in each pressure level (EC_j=1 in Eq.(22) for j=LP, MP, HP), a superheater in the low pressure level and a superheater in the high pressure level (SH_j=1 in Eq.(23) for j=LP,HP), two superheaters in the medium pressure level (SH_j=2 in Eq.(23) for j=MP), and a maximum value of 2 heat exchangers operating in parallel in each HRSG section (PE_i=2 in Eq.(21) $\forall i$).

Insert Figure 12

Figure 12 shows the obtained best configuration and the optimal operating conditions and sizes. Table 11 compares the number of heat exchangers involved in the Sabiya CCPP with that obtained in the optimal solution and the corresponding values of total heat transfer area required in each pressure level. Table 12 compares the contribution of each steam turbine to the desired electric power generation (125.39 MW). In Tables 11 and 12, the values of heat transfer area and electric power generated by each turbine of the Sabiya CCPP are calculated using the operating condition values reported in Almutairi et al. (2015) and the overall heat transfer coefficient values assumed in this study. In addition, the operating pressures in the three evaporators of the HRSG are the same as in Almutairi et al. (2015).

Regarding the HRSG configuration, Fig. 12 shows that the optimal solution requires 4 heat exchangers less than Almutairi et al. (2015) (10 vs. 14) and that the superheater in the LP level (6,LP) and the economizer in the HP level (6,HP) are arranged in parallel (section #6) while the remaining heat exchangers are arranged in series. The optimal configuration requires 245330 m^2 of heat transfer area, which represents by around 74% of that calculated for the Sabiya CCPP (331820 m^2).

The total mass flowrate of the working fluid in the steam cycle obtained in the current solution is slightly higher than that required in the Sabiya CCPP solution (99.5 kg/s vs. 96.55 kg/s). The flow rates of the streams leaving the HP, MP, and LP levels (#51, #34, and #12) in the current solution are 40.4 kg/s, 95.1 kg/s, and 4.4 kg/s, respectively, while those in the Sabiya CCPP solution are 74.6 kg/s, 88.36 kg/s, and 8.97 kg/s, respectively.

Table 11. Comparison of the number of heat exchangers and heat transfer area between the obtained optimal solution with a solution corresponding to a single block of the Sabiya CCPP (125.39 MW).

	Number of HEXs		Total heat transfer area (x10^3 m^2)	
	Sabiya CCPP (Almutairi et al., 2015)	This work	Sabiya CCPP (Almutairi et al., 2015)	This work
Economizers	5	3	189.25	113.49
Evaporators	3	3	107.14	88.89
Superheaters	6	4	35.42	42.95
Total	14	10	331.82	245.33

Table 22. Comparison of the electric power generated by steam turbines (125.39 MW per HRSG).

	Sabiya CCPP (Almutairi et al., 2015)	This work
Total net electric power (MW)	125.39	125.39
HP turbine	29.49	16.89
IP turbine	39.52	46.46
LP turbine	29.49	62.04

As shown in Table 12, the contribution of each steam turbine to the total electric power generation is different in both solutions. In the current solution, the largest contributor is the LP steam turbine with 62.04 MW, followed by the IP turbine with 46.46 MW. However, in the Sabiya CCPP solution, the largest contributor is the IP steam turbine with 39.52 MW, followed by the HP and LP steam turbines with 29.49 MW each.

Finally, it should be mentioned that the proposed approach of combining GDP with external routines for calculating the thermodynamic properties of fluids could be applied to other systems such as seawater desalination processes, cryogenic energy storage and air liquefaction, heat exchanger networks, water treatment processes, refrigeration processes. To this end, the first step is to develop a GDP model including the corresponding mass and energy balances as well as the sizing constraints. Then, the library containing the calculation of the thermodynamic properties of fluids is called from GAMS by using *$funclibin*. For other applications, it is possible to create new libraries (advanced user) or to use the wide variety of existing libraries (common user).

Beside the library IAPWS.dll employed in this work, the authors developed three general-purpose thermodynamic libraries that are available for their usage in the GAMS World Forum (https://forum.gamsworld.org/viewtopic.php?t=11547&p=27414). The former is called *RaoultLaw.dll* and is applicable for ideal solution. The second one is called *NRTLideal.dll* and includes the Nonrandom Two-Liquid (NRTL) activity coefficient model which is widely used in phase equilibrium calculations. And the third one is called *PengRobinson.dll* which includes the Peng Robinson equation of state. These libraries contain a database of 430 pure compounds.

6. Conclusions

A superstructure-based representation of three-pressure reheat combined-cycle power plants was conceived to derive a model of the process for simultaneous optimization of the configuration, design, and operation by applying generalized disjunctive programming and mixed-integer nonlinear programming formulations.

The optimization problem consisted in determining the way the heat exchangers and pumps of the heat recovery steam generator (HRSG) should be connected and the operating conditions and sizes of each process unit that minimize the total heat transfer area of the HRSG, while achieving a fixed, specified total net power generation level, given a flow rate and inlet temperature of the flue gas.

The superstructure model includes the possibility of selecting parallel, series, or combined parallel-series arrangements of heat exchangers in the hot, cold, and medium-temperature zones of the HRSG, as well as allowing the presence of more than one economizer and superheater at each pressure level. The inlet of the working fluid to the HRSG coming from the steam turbines for reheating can be located in the low-pressure level only, or in the low- and medium-pressure levels, or in all three pressure levels.

A model solution strategy based on a local search optimization algorithm based on the generalized reduced gradient was implemented in the General Algebraic Modeling System platform (GAMS). Extrinsic functions executed outside GAMS from dynamic-link libraries (DLL) – coded in the C programming language – were used to estimate the thermodynamic properties of the working fluids (flue gas and water/steam).

As a main result, improved process configurations of triple-pressure reheat HRSGs were obtained compared with respect to the reference cases reported in the literature.

The optimal solution obtained from the proposed superstructure was compared with a first reference case reported in the literature. Although the total heat loads in the HRSG in both studies are very similar (190.23 MW in the reference case and 192.14 MW in this work), the total heat transfer area required in this work is around 15% lower than the required in the reference case (91.74 m^2 vs. 107.70 m^2). This is due to the inclusion of 4 heat exchangers more than the reference case, making it possible to modify the configuration, include parallel exchanges along the HRSG, and obtain more appropriate driving forces in each heat exchanger. In both cases, the largest fraction of the generated power is produced by the low-pressure steam turbine and the smallest fraction by the high-pressure steam turbine.

Also, the optimal solution obtained from the proposed superstructure was compared with a second reference case corresponding to a single block of the existing Sabiya CCPP, located in Kuwait. For a same electric power generation (125.39 MW) and a total heat load in the HRSG (351.69 MW), the obtained optimal solution included 4 heat exchangers less (10 vs. 14) with a heat transfer area in the HRSG 26% less (245330 m^2 vs. 331820 m^2).

This paper contributes to the literature with a solution strategy and a GDP mathematical optimization model of natural gas combined-cycle power plants operated at three pressure levels and the corresponding solution strategy, and with novel configurations of HRSG.

The proposed model relies on the calculation of several properties of streams through thermodynamic models that have several parameters subject to uncertainties. Additionally, the overall heat-transfer coefficients are subject to uncertainties. The discussed optimal designs may vary with these uncertainties. Therefore, sensitivity and uncertainty analysis are required to identify when and which parameters play a significant role in the error propagation. To this end, random sampling techniques such as Monte Carlo (MC) will be considered in future works.

Acknowledgments

The *Consejo Nacional de Investigaciones Científicas y Técnicas* (CONICET) and the *Universidad Tecnológica Nacional-Facultad Regional Rosario* (UTN-FRRo) from Argentina are gratefully acknowledged for their financial support.

Notation

Sets

HE(i,j,k) contains the heat exchangers located in the section *i* and pressure level *j* with the stream *k*

EV(i) contains the sections where the evaporators are located.

PUMP(n,k,k') contains the pump number *n* with the corresponding inlet stream *k* and outlet stream *k´*

NHNP(i,j,n) contains the economizers located in the section *i* and pressure level *j* associated to the pump *n*

HNP(i,j,n) contains the heat exchangers located in the section *i* and pressure level *j* associated to the pump *n*

Indices

i sections of the heat recovery steam generator

j pressure levels in the heat recovery steam generator

k water stream number

n pump number

Positive Variables

A_{COND} Heat transfer area of the condenser in the Rankine cycle (m^2)

$A_{i,j}$ Heat transfer area of corresponding to the heat exchanger located in the section *i* and pressure level *j* (m^2)

h_i^G Enthalpy of the flue gas stream *G* in the section *i* (kJ kg^{-1})

h_k enthalpy of the stream *k* (kJ kg^{-1})

m_k mass flowrate of the stream *k* (kg s^{-1})

m^G mass flowrate of the flue gas stream *G* (kg s^{-1})

$Q_{i,j}$ heat load in the heat exchanger located in the section *i* and pressure level *j* (MW)

$\Delta T_{i,j}$ driving force corresponding to the heat exchanger located in the section *i* and pressure level *j* (K)

T_i^G temperature of the fluegas steam *G* in the section *i* (K)

T_k temperature of the stream *k* (K)

W net electrical power (MW)

$\Delta T_{i,j}$ driving force corresponding to the heat exchanger located in the section *i* and pressure level *j* (K)

Variables

THTA total heat transfer area (m^2)

Binary variables

$x_{i,j}$ existence of the heat exchanger in the section *i* and pressure level *j*

y_n existence of the pump *n*

z_k existence of the stream *k* associated to reheating

Parameter

EC_j maximum number of economizers operating in the pressure level *j*

PE_i maximum number of heat exchangers operating in parallel at the section *i*

SH_j maximum number of superheaters operating in the pressure level *j*

$U_{i,j}$ overall heat transfer coefficient (W m^{-2} K^{-1})

Acronyms

BARON	branch-and-reduce optimization navigator
CCPPs	combined-cycle power plants
CHP	combined heat and power
DLL	dynamic-link library
GA	genetic algorithms
GAMS	general algebraic modeling system
GDP	generalized disjunctive programming
HP	high pressure
HRSGs	heat recovery steam generators
IGCC	integrated gasification combined cycle
LP	low pressure
MINLP	mixed-integer nonlinear programming
MP	medium pressure
NGCC	natural gas combined cycle power plants
NLP	nonlinear programming
ORC	organic Rankine cycles
PUMP	pump
SA	simulated annealing
SBB	standard branch and bound
ST1	steam turbine 1
ST2	steam turbine 2
ST3	steam turbine 3

References

Ahadi-Oskui, T., Vigerske, S., Nowak, I., Tsatsaronis, G., 2010. Optimizing the design of complex energy conversion systems by Branch and Cut. Computers & Chemical Engineering 34 (8): 1226-1236. https://doi.org/10.1016/j.compchemeng.2010.03.007

Ahmadi, P., Dincer, I., 2011. Thermodynamic analysis and thermoeconomic optimization of a dual pressure combined cycle power plant with a supplementary firing unit. Energy Convers Manage 52(5), 2296–2308. https://doi.org/10.1016/j.enconman.2010.12.023

Ahmadi, P., Rosen, M.A., Dincer, I., 2012. Multi-objective exergy-based optimization of a polygeneration energy system using an evolutionary algorithm. Energy 46(1), 21–31.

https://doi.org/10.1016/j.energy.2012.02.005

Ahmetovic, E., Grossmann, I.E., 2011. Global superstructure optimization for the design of integrated process water networks. AIChE J 57, 434–457. https://doi.org/10.1002/aic.12276

Almutairi, A., Pilidis, P., Al-Mutawa, N., 2015. Energetic and Exergetic Analysis of Combined Cycle Power Plant: Part-1 Operation and Performance. Energies 8, 14118–14135; doi:10.3390/en81212418

Ameri, M., Mokhtari, H., Sani, M.M., 2018. 4E analyses and multi-objective optimization of different fuels application for a large combined cycle power plant. Energy 156, 371–386. https://doi.org/10.1016/j.energy.2018.05.039

Bakhshmand, S.K., Saray, R.K., Bahlouli, K., Eftekhari, H., Ebrahimi, A., 2015. Exergoeconomic analysis and optimization of a triple-pressure combined cycle plant using evolutionary algorithm. Energy 93, 555–567. https://doi.org/10.1016/j.energy.2015.09.073

Blumberg, T., Assar, M., Morozyuk, T., Tsatsaronis, G., 2017. Comparative exergoeconomic evaluation of the latest generation of combined-cycle power plants. Energy Convers Manage, 153, 616–626. https://doi.org/10.1016/j.enconman.2017.10.036

Bongartz, D., Najman, J., Mitsos, A, 2020. Deterministic global optimization of steam cycles using the IAPWS IF97 model. Optimization and Engineering 21, 1095-1131.https://doi.org/10.1007/s11081-020-09502-1

Boyaghchi, F., Molaie, H., 2015. Advanced exergy and environmental analyses and multi objective optimization of a real combined cycle power plant with supplementary firing using evolutionary algorithm. Energy 93, 2267–2279. https://doi.org/10.1016/j.energy.2015.10.094

Bracco, S., Siri, S., 2010. Exergetic optimization of single level combined gas–steam power plants considering different objective functions. Energy 35(12), 5365–5373. https://doi.org/10.1016/j.energy.2010.07.021

Brooke, A., Kendrick, D., Meeraus, A., 1992, GAMS: A User's Guide, Release 2.25. The Scientific Press, South San Francisco (CA).

Bruno, J.C., Fernandez, F., Castells, F., Grossmann, I.E., 1998. A rigorous MINLP model for the optimal synthesis and operation of utility plants. Chem Eng Res Des 76, 246–258. https://doi.org/10.1205/026387698524901

Bussieck, M., Drud, A., 2001. SBB: A New Solver for Mixed Integer Nonlinear Programming. http://ftp.gamsworld.org/presentations/present_sbb.pdf

Chen, J.J.J., 1987. Comments on improvements on a replacement for the logarithmic mean. Chem Eng Sci 42 (10), 2488 2489. http://dx.doi.org/10.1016/0009-2509(87)80128-8.

Chen, Q., Grossmann, I., 2019. Modern Modeling Paradigms Using Generalized Disjunctive Programming. Processes 7(11), 839. https://doi.org/10.3390/pr7110839

Drud A., 1992. CONOPT A Large-Scale GRG Code. Orsa Journal on Computing, 6, 207-216. https://www.gams.com/latest/docs/S_CONOPT.html

Elsido, C., Mian, A., Martelli, E., 2017. MINLP A systematic methodology for the techno-economic optimization of Organic Rankine Cycles. Energy Procedia 129, 26–33. https://doi.org/10.1016/j.egypro.2017.09.171

Faria, D.C., Bagajewicz, M.J., 2012. A new approach for global optimization of a class of MINLP problems with applications to water management and pooling problems. AIChE J 58, 2320–2335. https://doi.org/10.1002/aic.12754

Franco, A., Giannini, N., 2006. A general method for the optimum design of heat recovery steam generators. Energy 31, 3342–3361. https://doi.org/10.1016/j.energy.2006.03.005

Franco, A., Russo A., 2002. Combined cycle plant efficiency increase based on the optimization of the heat recovery steam generator operating parameters. Int J Therm Sci 41 (9), 843–859. https://doi.org/10.1016/S1290-0729(02)01378-9.

Gopalakrishnan, H., Kosanovic, D., 2015. Operational planning of combined heat and power plants through genetic algorithms for mixed 0–1 nonlinear programming. Comp Oper Res 56, 51–67. https://doi.org/10.1016/j.cor.2014.11.001

Grossmann, I., Lee, S., 2003. Generalized convex disjunctive programming: Nonlinear convex hull relaxation. Computational Optimization and Applications 26, 83-100. https://doi.org/10.1023/A:1025154322278

Grossmann, I., Ruiz, J., 2012. Generalized Disjunctive Programming: A Framework for Formulation and Alternative Algorithms for MINLP Optimization. The IMA Volumes in Mathematics and its Applications 154, 93–115. https://doi.org/10.1007/978-1-4614-1927-3_4

IAPWS R7-97, 2012. The International Association for the Properties of Water and Steam Lucerne, Switzerland August 2007 . http://www.iapws.org/relguide/IF97-Rev.pdf

Izyan, Z.N., Noryani, M., Dayanasari, A.H., Shuhaimi, M., 2014. MINLP model for simultaneous scheduling and retrofit of refinery preheat train. Inter J Energy and Environ 5 (2), 197-206.

Jing, R., Wang, M., Wang, W., Brandon, N., Li, N., Chen, J., Zhao, Y., 2017. Economic and environmental multi-optimal design and dispatch of solid oxide fuel cell based CCHP system. Energy Convers Manage 154, 365–379. https://doi.org/10.1016/j.enconman.2017.11.035

Kaviri, A.G., Jaafar, M.M.N., Lazim, T.M., 2012. Modeling and multi-objective exergy based optimization of a combined cycle power plant using a genetic algorithm. Energy Convers Manage 258, 94–103. https://doi.org/10.1016/j.enconman.2012.01.002

Kim, J.S., Edgar, T.F., 2014. Optimal scheduling of combined heat and power plants using mixed-integer nonlinear programming. Energy 77, 675–690. https://doi.org/10.1016/j.energy.2014.09.062

Lee, S., Grossmann, I.E., 2000. New algorithms for nonlinear generalized disjunctive programming. Comp Chem Eng 24 (9–10), 2125-2141. https://doi.org/10.1016/S0098-1354(00)00581-0

León, E., Martín, M., 2016. Optimal production of power in a combined cycle from manure based biogas. Energy Conversion and Management 114, 89-99. https://doi.org/10.1016/j.enconman.2016.02.002

Lu, B., Huang, S., Grossmann, I.E., 2017. Optimal Synthesis and Operation of Wastewater Treatment Process with Dynamic Influent. Ind Eng Chem Res 56 (30), 8663-8676. https://doi.org/10.1021/acs.iecr.7b01805

Manassaldi, J.I., Mussati, M.C., Scenna, N.J., Mussati, S.F., 2019. Development of extrinsic functions for optimal synthesis and design—Application to distillation-based separation processes. Comp Chem Eng 125, 532–544. https://doi.org/10.1016/j.compchemeng.2019.03.028

Manassaldi, J.I., Arias, A.M., Scenna, N.J., Mussati, M.C., Mussati, S.F., 2016. A discrete and continuous mathematical model for the optimal synthesis and design of dual pressure heat recovery steam generators coupled to two steam turbines. Energy 103, 807–823. https://doi.org/10.1016/j.energy.2016.02.129

Manassaldi, J.I., Mores, P.L., Scenna, N.J., Mussati, S.F., 2014. Optimal Design and Operating Conditions of an Integrated Plant Using a Natural Gas Combined Cycle and Postcombustion CO2 Capture. Ind Eng Chem Res 53, 17026–17042. https://doi.org/10.1021/ie5004637

Martelli, E., Elsido, C., Mian, A., Maréchal, F., 2017. MINLP Model and two-stage Algorithm for the Simultaneous Synthesis of Heat Exchanger Networks, Utility Systems and Heat Recovery Cycles. Comp Chem Eng 106, 663–689. https://doi.org/10.1016/j.compchemeng.2017.01.043

Mehrgoo, M., Amidpour, M., 2017. Configurations and pressure levels optimization of heat recovery steam generator using the genetic algorithm method based on the constructal design. Appl Therm Eng 122, 601–617. https://doi.org/10.1016/j.applthermaleng.2017.04.144

Mehrpanahi, A., Naserabad, S.N., Ahmadi, G., 2019. Multi-objective linear regression based optimization of full repowering a single pressure steam power plant. Energy 179, 1017–1035. https://doi.org/10.1016/j.energy.2019.04.208

Mores, P.L., Manassaldi, J.I., Scenna, N.J., Caballero, J.A., Mussati, M.C., Mussati, S.F., 2018. Optimization of the design, operating conditions, and coupling configuration of combined cycle power plants and CO2 capture processes by minimizing the mitigation cost. Chem Eng J 331, 870–894. https://doi.org/10.1016/j.cej.2017.08.111

Morosuk, T., Tsatsaronis, G., 2011. Comparative evaluation of LNG e based cogeneration systems using advanced exergetic analysis. Energy 36, 3771–3778. http://dx.doi.org/10.1016/j.energy.2010.07.035.

Mussati, S.F., Aguirre, P.A., Scenna, N.J., 2001. Optimal MSF plant design. Desalination 138, 341–347. https://doi.org/10.1016/S0011-9164(01)00283-1

Mussati, S.F., Aguirre, P.A., Scenna, N.J., 2003. Novel configuration for a multistage flash-mixer desalination system. Ind Eng Chem Res 42, 4828–4839. https://doi.org/10.1021/ie020318v

Mussati, S.F., Aguirre, P.A., Scenna, N.J., 2005. Optimization of alternative structures of integrated power and desalination plant. Desalination 2005; 182: 123–129. https://doi.org/10.1016/j.desal.2005.03.012

Mussati, S.F., Aguirre, P.A., Scenna, N.J., 2003. Dual-purpose desalination plants. Part II. Optimal configuration. Desalination 153, 185–189. https://doi.org/10.1016/S0011-9164(02)01126-8

Nadir, M., Ghenaiet, A., 2015. Thermodynamic optimization of several (heat recovery steam generator) HRSG configurations for a range of exhaust gas temperatures. Energy 86, 685–695. https://doi.org/10.1016/j.energy.2015.04.023

Naserabad, N.S., Mehrpanahi, A., Ahmadi, G., 2018. Multi-objective optimization of HRSG configurations on the steam power plant repowering specifications. Energy 159, 277–293. https://doi.org/10.1016/j.energy.2018.06.130

Oliva, D.G., Francesconi, J.A., Mussati, M.C., Aguirre, P.A., 2011. Modeling, synthesis and optimization of heat exchanger networks. Application to fuel processing systems for PEM fuel cells. Int J Hydrogen Energy 36 (15), 9098-9114. https://doi.org/10.1016/j.ijhydene.2011.04.097

Pérez-Uresti, S.I., Martín, M., Jiménez-Gutiérrez, A., 2019. Superstructure approach for the design of renewable-based utility plants. Comp Chem Eng 123, 371–388. https://doi.org/10.1016/j.compchemeng.2019.01.019

Rezaie, A., Tsatsaronis, G., Hellwig, U., 2019. Thermal design and optimization of a heat recovery steam generator in a combined-cycle power plant by applying a genetic algorithm. Energy 168, 346–357. https://doi.org/10.1016/j.energy.2018.11.047

Sahoo, P.K., 2008. Exergoeconomic analysis and optimization of a cogeneration system using evolutionary programming. Appl Therm Eng 28, 1580–1588. https://doi.org/10.1016/j.applthermaleng.2007.10.011

Santos, M.I., Uturbey, W., 2018. A practical model for energy dispatch in cogeneration plants. Energy 151, 144–159. https://doi.org/10.1016/j.energy.2018.03.057

Sahinidis, N.V., 2000. BARON Branch And Reduce Optimization Navigator. https://www.gams.com/latest/docs/S_BARON.html

Taccari, L., Amaldi, E., Martelli, E., Bischi, A., 2015. Short-Term Planning of Cogeneration Power Plants: a Comparison Between MINLP and Piecewise-Linear MILP Formulations. Computer Aided Chemical Engineering 37, 2429–2434. https://doi.org/10.1016/B978-0-444-63576-1.50099-6

Tanvir, M.S., Mujtaba, I.M., 2008. Optimisation of design and operation of MSF desalination process using MINLP technique in gPROMS. Desalination 222, 419–430. https://doi.org/10.1016/j.desal.2007.02.068

Tsatsaronis, G., Park, M.H., 2002. On avoidable and unavoidable exergy destructions and investment costs in thermal systems. Energy Convers Manage, 43, 1259–1270. http://dx.doi.org/10.1016/S0196-8904(02)00012-2.

Tsatsaronis, G, 1999. Strengths and limitations of exergy analysis. Thermodynamic Optimization of Complex Energy Systems. NATO Science Series (Series 3. High Technology), 69, 93–100. https://doi.org/10.1007/978-94-011-4685-2_6

Vecchietti, A., Lee, S., Grossmann, I.E., 2003. Modeling of discrete/continuous optimization problems: characterization and formulation of disjunctions and their relaxations. Comp Chem Eng 27 (3), 433-448. https://doi.org/10.1016/S0098-1354(02)00220-X

Wang, L., Yang, Y., Dong, C., Morozyuk, T., Tsatsaronis, G., 2014. Parametric optimization of supercritical coal-fired power plants by MINLP and differential evolution. Energy Convers Manage 85, 828–838. https://doi.org/10.1016/j.enconman.2014.01.006

Zhang, J., Liu, P., Zhou, Z., Ma, L., Li, Z., Ni, W., 2014. A mixed-integer nonlinear programming approach to the optimal design of heat network in a polygeneration energy system. Appl Energy 114, 146–154. http://dx.doi.org/10.1016/j.apenergy.2013.09.057

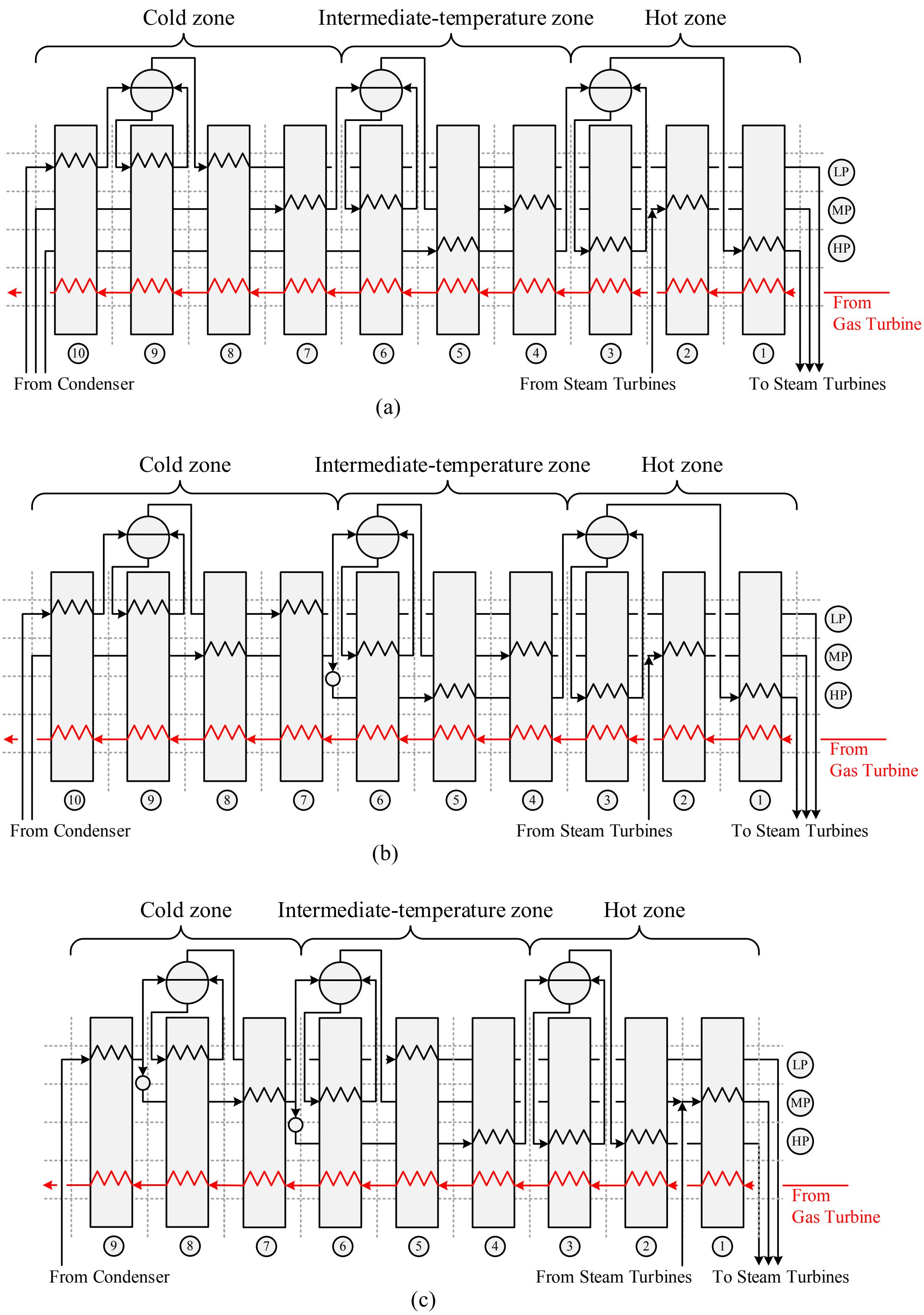

Figure 1. Three candidate HRSG configurations differing in the way of feeding the working fluid at the different pressure levels and in the location of some heat exchangers: (**a**) simultaneous feeds in the three pressure levels, (**b**) simultaneous feeds in the low pressure (LP) and medium pressure (MP) levels, (**c**) feed in the LP level.

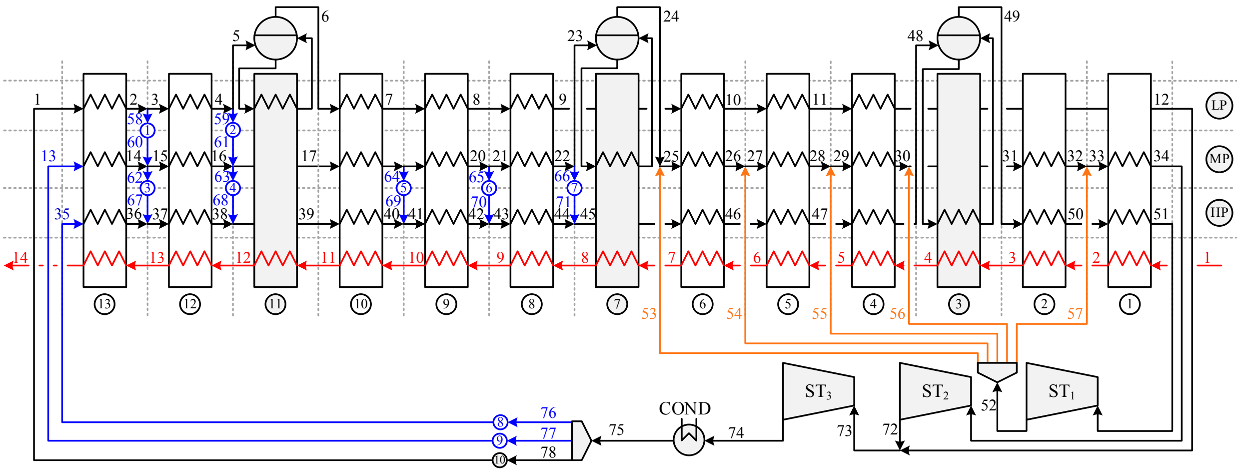

Figure 2. Process superstructure representation embedding many alternative HRSG configurations.

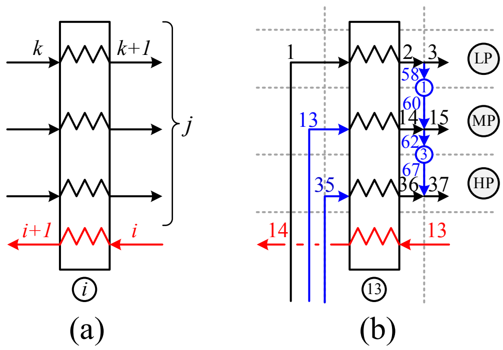

Figure 3. Representation and used nomenclature corresponding to a generic secton ‘i’ (**a**) and to the section i=13 as example (**b**).

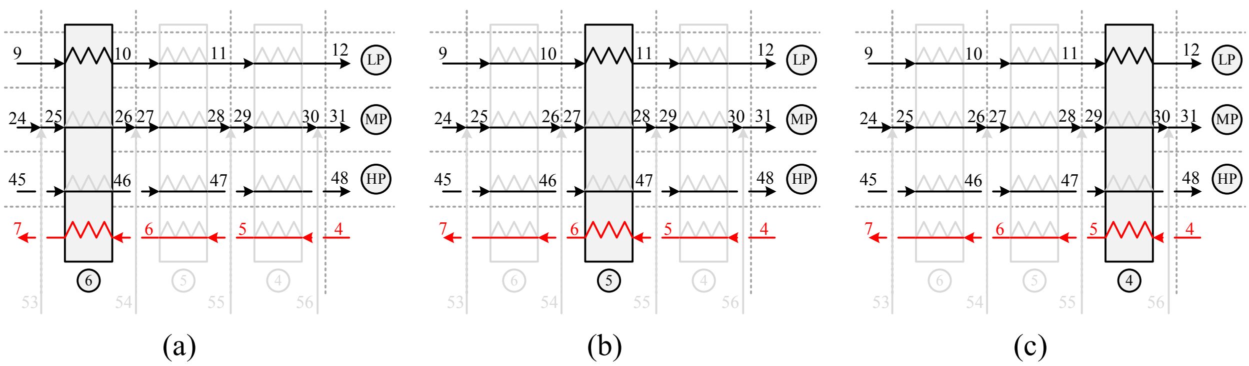

Figure 4. Equivalent solutions obtained when only one low-pressure (LP) superheater is selected in the sections i=4, 5, and 6.

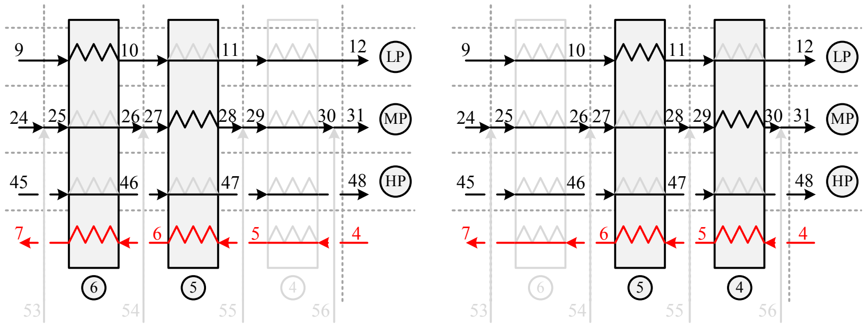

(a) (b)

Figure 5. Equivalent solutions obtained when two heat exchangers are selected from the sections i=4, 5, and 6 and at the low-pressure (LP) and medium-pressure (MP) levels.

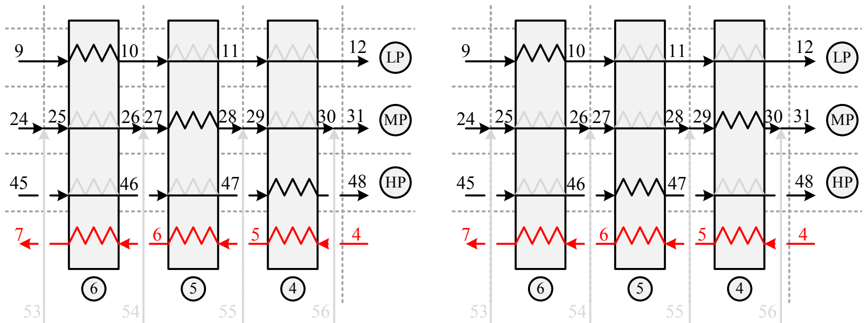

(a) (b)

Figure 6. Different (no equivalent) solutions obtained when three heat exchangers are selected from the sections i=4, 5, and 6.

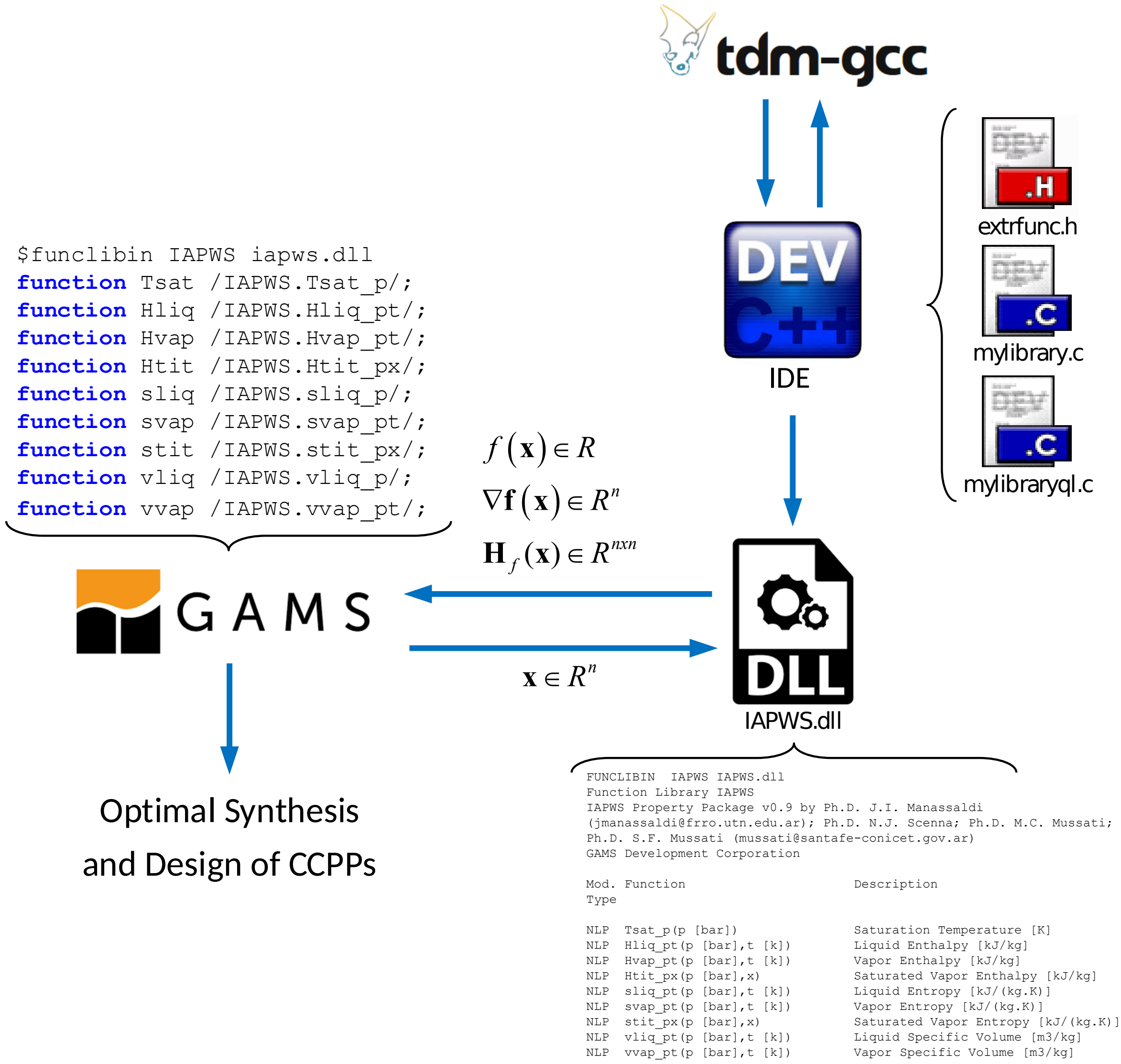

Figure 7. Main steps from the declaration to the execution of the extrinsic functions.

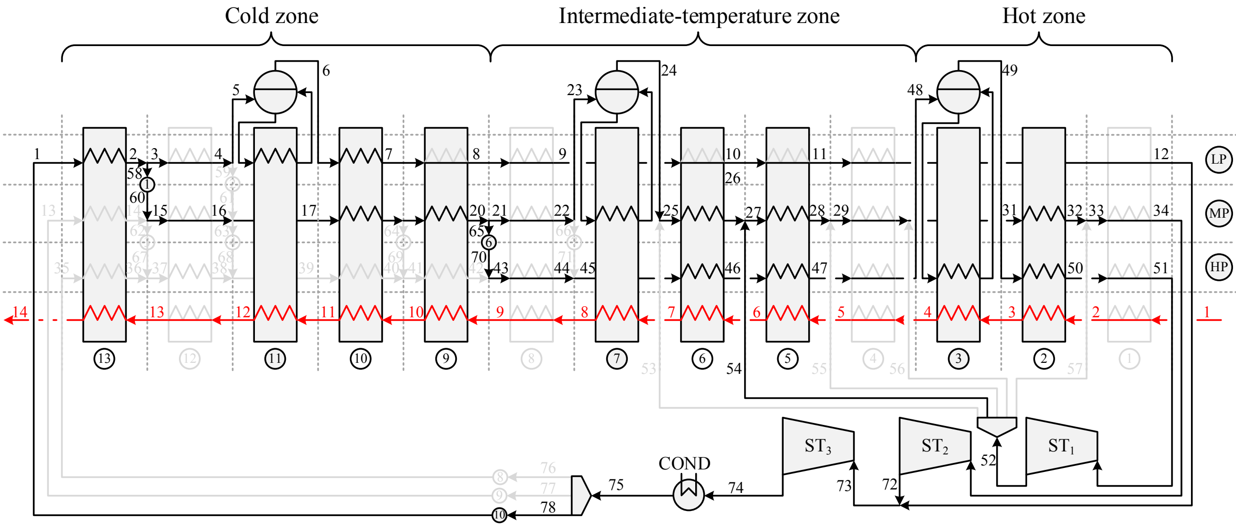

Figure 8. RC solution. Optimal configuration discussed in Franco and Giannini (2006).

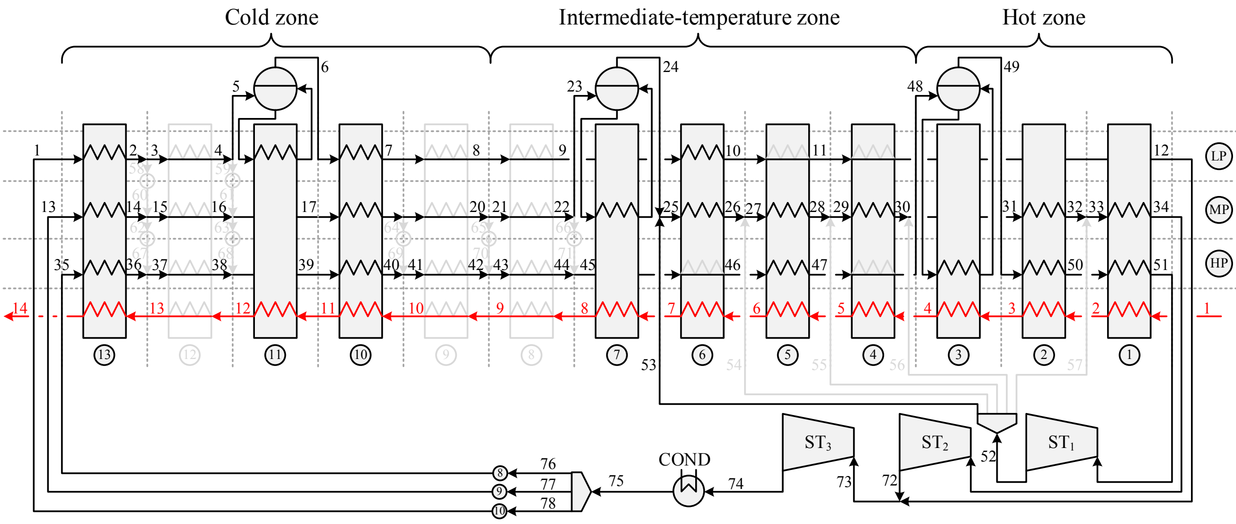

Figure 9. OS solution. Optimal configuration obtained considering the possibility of using parallel heat exchangers and repetition of economizers and superheaters at the same pressure level.

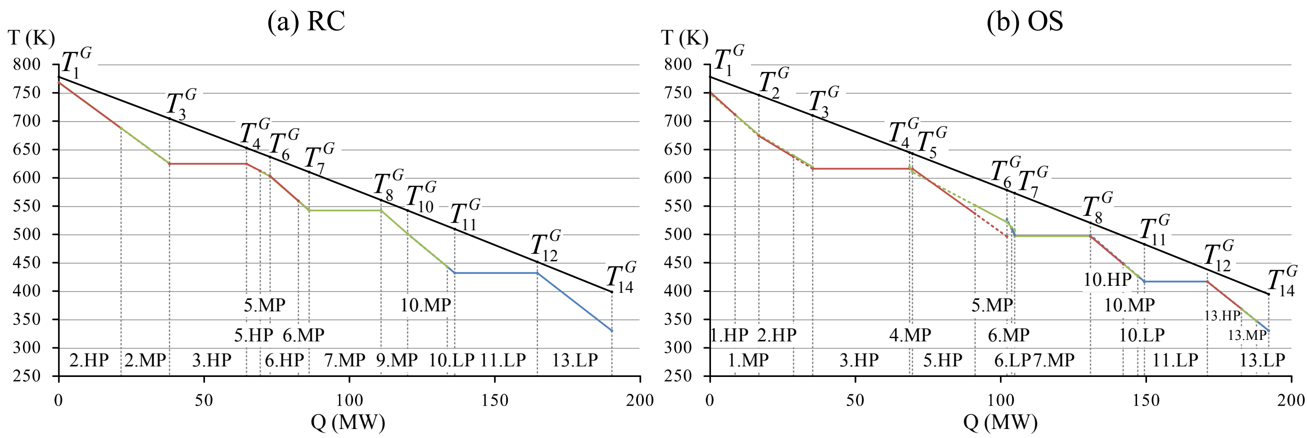

Figure 10. Temperature-enthalpy (T-H) diagram obtained for each configuration: (**a**) RC (Franco and Giannini, 2006), (**b**) OS (this work).

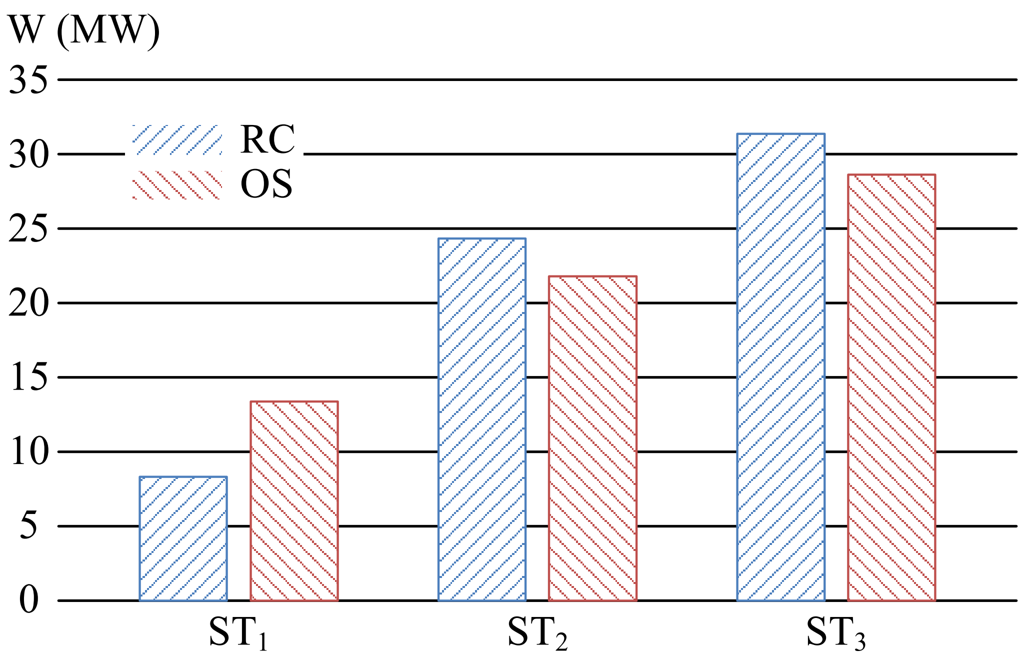

Figure 11. Comparison of the optimal electric power generated in each steam turbine in the configurations RC and OS.

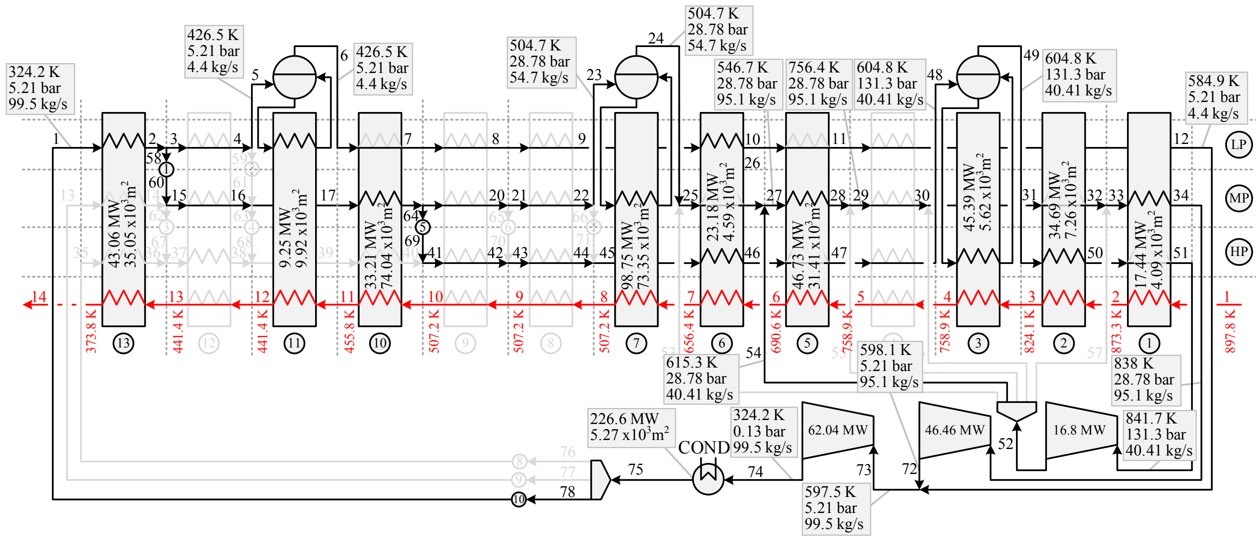

. **Figure 12**. Optimal solution obtained for design specifications corresponding to the Sabiya combined-cycle power plant (Almutairi et al., 2015).

Figure captions

Figure 1. Three candidate HRSG configurations differing in the way of feeding the working fluid at the different pressure levels and in the location of some heat exchangers: (**a**) simultaneous feeds in the three pressure levels, (**b**) simultaneous feeds in the low pressure (LP) and medium pressure (MP) levels, (**c**) feed in the LP level.

Figure 2. Process superstructure representation embedding many alternative HRSG configurations.

Figure 3. Representation and used nomenclature corresponding to a generic secton 'i' (**a**) and to the section i=13 as example (**b**).

Figure 4. Equivalent solutions obtained when only one low-pressure (LP) superheater is selected in the sections i=4, 5, and 6.

Figure 5. Equivalent solutions obtained when two heat exchangers are selected from the sections i=4, 5, and 6 and at the low-pressure (LP) and medium-pressure (MP) levels.

Figure 6. Different (no equivalent) solutions obtained when three heat exchangers are selected from the sections i=4, 5, and 6. .

Figure 7. Main steps from the declaration to the execution of the extrinsic functions.

Figure 8. RC solution. Optimal configuration discussed in Franco and Giannini (2006).

Figure 9. OS solution. Optimal configuration obtained considering the possibility of using parallel heat exchangers and repetition of economizers and superheaters at the same pressure level.

Figure 10. Temperature-enthalpy (T-H) diagram obtained for each configuration: (**a**) RC (Franco and Giannini (2006)), (**b**) OS (this work).

Figure 11. Comparison of the optimal electric power generated in each steam turbine in the configurations RC and OS.

Figure 12. Optimal solution obtained for design specifications corresponding to the Sabiya combined-cycle power plant (Almutairi et al., 2015) .

Author statement

Juan I. Manassaldi: Modeling, Methodology, Software, Visualization.

Miguel C. Mussati: Conceptualization, Discussion of Results, Writing - original draft.

Nicolas J. Scenna: Conceptualization, Discussion of Results, Draft review.

Sergio F. Mussati: Conceptualization, Discussion of Results, Writing - review & edition, Supervision.